A hierarchically correlated flow defect model for metallic glass: Universal understanding of stress relaxation and creep

Q. Hao[a], G.J. Lyu[b], E. Pineda[c], J.M. Pelletier[d], Y.J. Wang[b,e], Y. Yang[f,g], J.C. Qiao[a,*]

[a]School of Mechanics, Civil Engineering and Architecture, Northwestern Polytechnical University, Xi'an 710072, China

[b]State Key Laboratory of Nonlinear Mechanics, Institute of Mechanics, Chinese Academy of Sciences, Beijing 100190, China

[c]Department of Physics, Institute of Energy Technologies, Universitat Politècnica de Catalunya - BarcelonaTech, 08019 Barcelona, Spain

[d]Université de Lyon, MATEIS, UMR CNRS5510, Bat. B. Pascal, INSA-Lyon, F-69621 Villeurbanne Cedex, France

[e]School of Engineering Science, University ofChinese Academy of Sciences, Beijing 100049, China

[f]Department of Mechanical Engineering, College of Engineering, City University of Hong Kong, Tat Chee Avenue, Kowloon Tong, Kowloon, Hong Kong SAR, China

[g]Department of Materials Science and Engineering, College of Engineering, City University of Hong Kong, Tat Chee Avenue, Kowloon Tong, Kowloon, Hong Kong SAR, China

Submitted to International Journal of Plasticity

* Corresponding author: Prof. Dr. J.C. Qiao (qjczy@nwpu.edu.cn)

Abstract

Due to the structurally disordered arrangement of atoms and deviation from thermodynamic equilibrium, the physical and mechanical properties of metallic glasses can vary with time, temperature and magnitude of strain or stress. The current work provides a theoretical framework based on the hierarchically correlated atomic theory, which allows a quantitative description of the non-elastic deformation in metallic glasses. The defect concentration is adopted as an order parameter, which can evolve with temperature and non-elastic strain owing to correlated atomic movements. Through our hierarchically correlated atomic theory, we derive the characteristic times for local shear events in metallic glasses that entail activation, growth and/or annihilation of flow defects, which however are not accounted for in the previous mean field theories. Finally, we demonstrate that the current theoretical framework can be validated by the stress relaxation and creep experiments on typical La-based metallic glasses, which in turn provides quantitative insights into the non-elastic deformation mechanisms in metallic glasses.

Keywords:
Metallic glass; Stress relaxation; Creep; Non-elastic deformation

1. Introduction

Metallic glasses (MGs), as a relatively newcomer of glassy materials, are of interest and significance in materials science, condensed matter physics, and engineering benefitting from their exceptional physical, chemical, and mechanical properties. The superior properties include but not limited to high strength and hardness, high elastic limit and excellent corrosion resistance (Inoue and Takeuchi, 2011; Khmich et al., 2021; Wang, 2012). Unfortunately, engineering applications of these materials as structural materials are limited due to the tendency of shear localization and macroscopically brittle fracture at ambient temperature (Sun et al., 2016; Zhou et al., 2013). It is well documented that at low temperature ($T < 0.8\,T_g$) and with sufficiently high stress, the deformation is not homogeneous but takes place locally with quite higher magnitude than the average value. Here T_g is the glass transition temperature. On the other hand, at high temperature ($T > 0.8\,T_g$) the non-elastic deformation is rather homogeneous in the glassy solids, which results in a large plastic stability (Argon, 1979; Cheng et al., 2021a). In fact, the strongly temperature-dependent mechanical behaviors of glassy solids do not merely reflect in the non-elastic deformation. For example, when temperature is below T_g, the shear modulus of metallic glass in the glassy state is of the order of tens to hundreds GPa. It drastically decreases by several orders of magnitude above T_g, where the glass-forming system stays in its supercooled liquid region (SLR). Under such conditions, the mechanical response of metallic glasses is very sensitive to temperature as well as strain rate, which should be considered in both theoretical research and engineering application.

These unique features of metallic glasses are essentially related to their metastable

structural features of long-range disorder and short-range order, which is obtained by quenching from the melt (Qiao et al., 2019a). The constituent atoms of the traditional crystalline alloys are arranged in three-dimensional space in a periodic manner. The real crystalline material actually contains a number of defects which can be classified as point (interstitials and vacancies), line (different types of dislocations) and planar (grain boundaries and stacking faults) types. However, the random arrangement of atoms in metallic glasses raises a problem about how to describe their microstructure. Therefore, understanding and characterizing the disordered atomic structure in metallic glasses is one of the key topics and challenging issues in the community of materials science. Intuitively, it seems easy to hypothesize that the structure of metallic glasses is continuous and uniform at continuum level because it is isotropic and homogeneous at the macroscopic level. However, with continuous advance in development of experimental techniques of structural characterization (Liu et al., 2011; Nomoto et al., 2021; Yang et al., 2021; Zhu et al., 2018), as well as atomic-level computer simulations (Cheng and Ma, 2011; Tang and Harrowell, 2013), the atomic structure of metallic glasses has been considered to contain structural heterogeneities at nano-scale, which appears as a frozen-in structural feature inherited from the equilibrium super-cooled liquid (Afonin et al., 2019; Qiao et al., 2019c; Song et al., 2021; Zhang et al., 2018). Therefore, versatile types of structural defects, e.g., these termed as flow units (Wang and Wang, 2019; Zhu et al., 2013), free volume (Turnbull and Cohen, 1970), shear transformation zone (Argon, 1979; Falk and Langer, 1998; Langer, 2015; Van Loock et al., 2021), interstitials (Granato, 2014; Mitrofanov et al., 2016) and quasi-point defects (Cheng et al., 2021b; Perez, 1990), have been proposed based on fluctuations of local density, enthalpy and entropy in amorphous solids.

How to establish the correlation between microstructure (defect) and deformation mechanism is important and still an unsolved issue since it remains challenging to incorporate the microscopic mechanisms such as atomic movements into the constitutive model for the macroscopic plastic deformation (Hufnagel et al., 2016; Jiang et al., 2020; Lin et al., 2020; Ruan et al., 2022). We can refer to a kind of established method of crystal plasticity model describing the deformation behavior of crystals, which is usually based on the Orowan equation with significant role of dislocation kinetics (McElfresh et al., 2021; Po et al., 2016; Stukowski et al., 2015; Yu et al., 2021). The plastic strain rate is directly associated with the multiplication and annihilation process of dislocations through the dislocation density. These models can better reflect a clear physical picture, that is, dislocation is the main carrier of plastic deformation. The relevant model parameters have clear physical meanings and can be obtained from either experiments or atomistic simulations, which makes these models be widely applicable (Arsenlis and Parks, 2002; Li et al., 2021). Consequently, the basic concept of crystal plasticity model can be used as a starting point of the endeavor in establishment of deformation model for metallic glass.

Based on the earlier free volume model for liquid transport developed by Cohen

and Turnbull (Turnbull and Cohen, 1970), Spaepen (Spaepen, 1977) proposed a microscopic mechanism for steady state inhomogeneous flow in metallic glass by taking free volume as an order parameter, which involves two competing processes: a stress-induced disordering and a diffusion controlled reordering process. Then a theory is presented by Argon (Argon, 1979; Argon and Kuo, 1979) for plastic deformation of metallic glasses based on two modes of thermally activated shear transformations initiated around the free volume regions under the operation of applied shear stress, which predicts the very rapid shear localization at low temperatures. Falk and Langer (Falk and Langer, 1998) defined the fundamental deformation unit undergoing local shear rearrangement as the shear transformation zone (STZ) in a study of deformation behavior of metallic glasses using molecular dynamics simulations. Huang et al. (Huang et al., 2002) provided a general framework in the context of continuum mechanics, and successfully simulated the development of the inhomogeneous deformation and the strain localization with free volume concentration as the internal variable. It should be noted that the STZ theory is essentially a mean-field model, which regards the density and orientations of local flow defects as dynamic variables, and does not describe the correlation between different STZs in its present form (Langer, 2015). In addition, the transition from jamming to flow in the plastic yield process is controlled by applied stress. The pre-yielding deformation was a trivial elastic process for stress below the yield stress; yielding occurs once STZs creation is activated at stress that exceeds the yield stress. However, some experiments have showed that MGs undergo anelastic or permanent deformation even at room temperature (Huo et al., 2013; Ye et al., 2010). A core-shell model was proposed by Yang et al. (Ke et al., 2014; Yang et al., 2012a) to rationalize the pre-yielding deformation, which can explain the anelastic deformation by considering the elastic back-stress from solid-like atoms.

In view of the proceeding facts, we cannot help but wonder what the internal relationship between the microscopically structural defect, deformation unit and macroscopic non-elastic deformation is in metallic glasses. When stress is applied, the deformation unit first being activated is selected from many potential sites in a metallic glass. It is easy to envision that the defect sites with high free energy and large atomic mobility are easier to be activated to produce atomic rearrangement (Johnson and Samwer, 2005; Lei et al., 2020; Wang and Wang, 2019). As described in the literature (Argon and Shi, 1983; Atzmon and Ju, 2014; Qiao et al., 2019b), these deformation units are isolated spatially at low strain, and the deformation carried by them is reversible and recoverable (anelastic deformation) after removal of stress. For longer time of application of stress, the size of the deformation unit might reach a limit value for which the boundary bordering it will be extended such that it will encounter neighboring deformation units and lose its integrity. The resultant deformation is irreversible (plastic deformation).

Based on the above analysis, the current work aims to provide a physics-informed model, which considers the determination of the atomic mobility through the concept

of hierarchically correlated movements proposed by Palmer et al. (Palmer et al., 1984), and the correlation between the evolution of deformation units and the macroscopic non-elastic deformation. The physical model will be used to establish a universal understanding between the small-strain linear viscoelastic dynamic mechanical response and the large-strain plastic deformation behavior (uniaxial tension and creep). A convincing validation is performed on a $La_{60}Ni_{15}Al_{25}$ metallic glass by comparison between the experimental measurements and the theoretical prediction. In addition, the present framework is also extended to decipher the evolution of characteristic times of α and β relaxation processes in metallic glass, therefore intuitively explaining the two-step stress relaxation phenomenon from a theoretical perspective.

2. Experiments

2.1. Specimen preparation

The alloy ingots with nominal composition $La_{60}Ni_{15}Al_{25}$ (at. %) were prepared by the arc-melting method in a pure Ar atmosphere. All the alloy ingots were flipped and re-melted at least six times to guarantee chemical homogeneity, and then the molten liquid was sucked into a water-cooled copper mold to obtain an alloy plate with dimensions of 85 mm (length) × 10 mm (width) × 2 mm (thickness). Glassy ribbons with an approximate 50 μm thickness were produced using a classical melt-spinning method under argon atmosphere. The amorphous nature was ascertained by X-ray diffraction (XRD). The glass transition temperature $T_g = 453$ K and the onset crystallization temperature $T_x = 505$ K were measured at a heating rate of 3 K min^{-1} by a DSC 404, NETZSCH.

can be and differential scanning calorimetry (DSC).

2.2. Dynamic mechanical analysis (DMA)

The temperature-dependent, time-dependent and frequency-dependent dynamic mechanical properties of $La_{60}Ni_{15}Al_{25}$ MG have been investigated extensively in previous works (Jiang et al., 2016; Qiao et al., 2015). Here, as a powerful tool to study dynamic mechanical properties of glassy solids, Dynamic mechanical analysis experiments were performed by a commercial DMA apparatus (TA instruments Q800) in a single cantilever mode. Testing specimens with dimensions of 30 mm (length) × 2 mm (width) × 1 mm (thickness) were cut by an electric discharge machine, and then the surfaces of test samples were polished by emery paper prior to the DMA experiments. The basic principle of DMA can be simply described as applying a sinusoidal stress (or strain) to the sample and analyzing the response of the material to this mechanical stimulation. The complex modulus $E^* = E' + iE''$ (E' is the storage modulus and E'' the loss modulus), is obtained from the material's response to the oscillating force. The tangent of the phase angle, one of the most important key parameters measured by DMA, could be determined as $\tan\delta = E''/E'$. The detailed

information about dynamic moduli and the DMA apparatus were described in the previous literatures (Etienne et al., 1982; Menard, 2015). The temperature scans were performed at a constant heating rate of 3 K/min with a set of given driving frequencies. The frequency scans at different temperatures were performed at the frequency range from 0.01 to 2 Hz. The master curve with a large frequency window can be obtained based on the time-temperature-superposition (TTS) principle, as described in previous literatures (Ferry, 1980; Olsen et al., 2001). Indeed, the frequency scans were carried out in MATEIS laboratory of INSA Lyon. The evolution of the storage and loss dynamic shear moduli were obtained using the home-made low frequency inverted torsion pendulum apparatus in a high vacuum atmosphere.

2.3 Uniaxial tensile tests and creep

The uniaxial tensile tests were performed at 430 K under strain rate of 3×10^{-4} s^{-1}, using the strain rate mode of a TA Q800 DMA equipment. The creep tests were carried out in the creep mode of DMA machine at given temperatures and stress. The samples were heated to measure temperature with a heating rate of 10 K/min, and the samples were held for 10 min to ensure thermal equilibration prior to tensile or creep tests.

3. Theory

3.1 Concept of defect sites

In analogy to the crystalline metals, the physical and mechanical properties of metallic glasses are thought to be closely related to some kind of structural defects. In a metallic glass, the random close packed arrangement of atoms leads to some relatively "loose" and "dense" sites, which has been observed extensively by experiments and numerical simulations (Feng et al., 2016; Tsai et al., 2017; Yang et al., 2012b). A loose or dense site may be regarded as a defect, which corresponds to extra free volume or anti-free volume. Compared with crystals, one can consider that the defects of amorphous materials are equivalent to distributed "vacancies" or "interstitials". Computer simulations of atomic arrangements in the amorphous system strengthen this picture of structure (Srolovitz et al., 1981). So the concept of "quasi-point defects" appears richer than that of "free volume". As previously reported, the free volume model was conceived for a hard-sphere system, and do not apply well for metallic system (Egami et al., 2013).

These defects or structural fluctuations are already present in the supercooled liquid and become frozen-in during the quenching of the melt. It should be noted that the defects thus defined are the sites where fluctuations of density occur. Although the density fluctuations can be either positive (anti-free volume) or negative (free volume), the defects correspond to positive fluctuations of enthalpy and entropy in all cases. Perez et al. (Perez, 1990) defined these sites formed by a structural unit and its first

neighbors as quasi-point defects (QPD), whose enthalpy and entropy are higher than the average value of system.

The physical aspects of the structural defects of amorphous materials have been described by the concepts proposed by Egami (Egami, 1981, 2011), Spaepen (Spaepen, 1978) and Srolovitz et al. (Srolovitz et al., 1981). In the supercooled liquid, one can determine the variation of defect concentration C_{d} with temperature

$$C_{\mathrm{d}} = \frac{1}{1 + \exp(-\Delta S_{\mathrm{F}}/k)\exp(\Delta H_{\mathrm{F}}/kT)} \quad (1)$$

where ΔH_{F} and ΔS_{F} are the enthalpy and entropy of a QPD formation. In the glassy state, i.e. $T < T_{\mathrm{g}}$, the defects are frozen and their concentration is constant that is equal to $C_{\mathrm{d}}(T_{\mathrm{g}})$ if excluding any structural relaxation. It should be pointed out that unlike the defects in crystals (point defects, dislocation and grain boundary) that can be well defined for their own identity, the defects in metallic glasses are quite difficult to be defined and characterized. In addition, a kind of defects in crystals have the same character length, but the characteristic size in metallic glasses would rather follow a statistical distribution. Therefore, it is difficult to give the specific character length of these defects in metallic glasses by defining some cut-off in the continuous distribution of some structural parameter. As a result, it usually adopts a mean-field description of defect concentration in amorphous materials, e.g., the shear transformation model (Falk and Langer, 1998), the free volume model (Spaepen, 1977), and cooperative shear model (Johnson and Samwer, 2005), etc. The structural heterogeneity and heterogeneous dynamic feature, such as distribution of energy barrier for local structural excitations, is considered in the present model by assuming identical geometry of defect but varied dynamic features represented by different relaxation times.

3.2 Atomic mobility and hierarchical correlation effects

Under a stress field, the deformation of MGs may be either elastic, anelastic or plastic, suggesting different types of motions of structural units within the material. Therefore, understanding the essence of atomic or molecular motion at microscale of amorphous solids is important to explain the various macroscopic properties.

Palmer et al. (Palmer et al., 1984) considered that the motion of structural units in amorphous materials was hierarchically constrained, that is, the most mobile structural unit ‘jumps’ first, and it is followed by less rapid movements. The total duration of a certain motion is equal to the sum of the time consumed by all previously activated structural units. In this framework, a theoretical model for relaxation in strongly interacting glassy materials was proposed (Palmer et al., 1984). This model is based on a scenario of hierarchically constrained dynamics between different degrees of freedom. There is a discrete series of levels, $n = 1, 2, \ldots$, and the degrees of freedom of level n is represented by N_n Ising spins. Each spin in level $n + 1$ can only change its state if μ_n

spins in level n ($\mu_n \leq N_n$) obtain one particular state among the 2^{μ_n} possible ones. Therefore, the duration of the change of state in level n will be given by

$$\tau(n) = \tau(n-1) \cdot 2^{\mu_{n-1}} = \cdots = \tau(1) \cdot \exp\left(\sum_{z=1}^{n-1} \mu_z \cdot \ln 2\right) \tag{2}$$

The μ_n is at most 5 or 10 due to the constrained atomic motion but could be less than 1 to imply the weak constraint. In addition, it should be considered that $\tau(n)$ attains a large but finite value $\tau_{\max}$ for $n \to \infty$, thus the authors have postulated that the parameter μ_n should decrease with n rapidly enough for $\sum \mu_n$ to converge. Perez et al. (Perez et al., 1988) have particularly considered the following possibility:

$$\mu_z \cdot \ln 2 = \mu_1 \cdot z^{-p} = \mu_1 \cdot z(t_z/t_0)^{-p} \tag{3}$$

where z is the integral number and p is higher but close to 1. Therefore, the characteristic time corresponding to excitation in the nth level ($n = t/t_0$) can be given by

$$\tau(t) = \tau(1) \cdot \exp\left(\mu_1 \sum (t_z/t_0)^{-p}\right) \tag{4}$$

In the limiting case (replacing the sum by the integral), Eq. (4) can be written as:

$$\tau(t) = \tau(1) \cdot \exp\left(\mu_1 \frac{1 - n^{1-p}}{p-1}\right) \tag{5}$$

where $0 < \mu_1 < 1$ is the structural parameter reflecting the correlation effects between the different atomic motions. $\mu_1 = 0$ corresponds to a situation the correlation effects can be negligible. $\mu_1 = 1$ reflects the most extreme correlation effects. Taking the limit of Eq. (5) at $p = 1^+$, one can get:

$$\tau(t) = \tau(1) \cdot (t/t_0)^{\mu_1} \tag{6}$$

Moreover, we should consider that that $\tau(t)$ attains a finite value $\tau_{\max}$ for $t \to \infty$. By taking into account the condition $\tau(t) = \tau_{\max}$ when $t = \tau_{\max}$, we may thus write:

$$\tau(t) = \tau(1) \cdot (t/t_0)^{\mu_1}, \qquad \text{for } \tau(1) < t < \tau_{\max} \tag{7.a}$$

$$\tau(t) = \tau_{\max} = (\tau(1)/{t_0}^{\mu_1})^{1/1-\mu_1}, \quad \text{for } t > \tau_{\max} \tag{7.b}$$

In the above series of derivations, $\tau(1)$ is regarded as the characteristic time of an elementary motion which can be replaced by the characteristic time τ_β of the β relaxation process. It is well accepted that τ_β varies with temperature T according to the Arrhenius law:

$$\tau_\beta = \tau(1) = \tau_{\beta 0} \exp\left(\frac{U_\beta}{kT}\right) \tag{8}$$

where the $\tau_{\beta 0}$ is the pre-exponential factor and U_β is the apparent activation energy of an elementary motion. Eq. (8) describes the β relaxation as a thermally activated

process. In fact, under high stress, a thermomechanical coupling activation should be considered and the energy barrier of activation can be reduced by the mechanical work (Boyce et al., 1988; Perez, 1984; Schuh et al., 2005). In order to introduce the contribution of stress during the β relaxation activation, Eq. (8) was modified as (Pelletier et al., 2000; Rinaldi et al., 2011):

$$\tau_\beta = \tau_{\beta 0} \exp\left[\frac{U_\beta \left(1 - \frac{\sigma}{\sigma_1}\right)^{3/2}}{kT}\right] \tag{9}$$

where σ_1 is the value of stress which enables the energy crossover at 0 K. No thermal fluctuation is necessary for crossing the energy barrier when σ is equal to σ_1. Crossing the barrier is therefore a complete mechanical, or athermal process. The exponent "3/2" in the Eq. (9) is obtained by considering the sinusoidal profiles of energy barrier and the corresponding parabolic force.

It is noticeable that the intensity of correlation effects is closely related to the concentration of defects. The higher the C_d, the weaker the correlation effect becomes. In the literature (Perez, 1998), Perez et al. consider $0 < \chi < 1$ as a structural parameter characterizing the correlation effect ranging from full order ($\chi = 0$) to full disorder ($\chi = 1$). χ increases with increasing disorder of system and therefore also increases with the concentration of defects. Its value is equal to a constant times C_d when the temperature is close to T_g. We therefore have:

$$\chi = 1 - \mu_1 = \text{const} \cdot C_d \tag{10}$$

Thus Eq. (7) can be written as:

$$\tau(t) = \tau_\beta \cdot (t/t_0)^{1-\chi}, \qquad \text{for } \tau_\beta < t < \tau_{\max} \tag{11.a}$$

$$\tau(t) = \tau_{\max} = \left(\tau_\beta / {t_0}^{1-\chi}\right)^{1/\chi}, \quad \text{for } t > \tau_{\max} \tag{11.b}$$

3.3 Mechanism of deformation

As discussed in previous literature (Argon, 1979; Li et al., 2013; Schall et al., 2007; Xu et al., 2018), the macroscopic non-elastic deformation is accommodated by the mechanism of cooperative shearing of atomic clusters, which termed shear transformation zones (STZs). At small strain, STZs are isolated and the deformation is recoverable (anelasticity) from the instant removal of stress. For longer time with application of stress, the expansion of STZs might result in the case that their boundaries begin to interact with each other, cancelling the elastic energy. The resultant deformation would be permanent and irreversible (plasticity). According to the previous physical model (Perez, 1998), atomic clusters accommodating anelastic deformation might be identified as sheared microdomains (SMDs). The sites of nucleation of SMDs are the sites of defect described in the above section.

As shown in Fig. 1, the sites of defect are designated by yellow spherical symbols, which are potential activation sites of SMDs. On the first stage of deformation, the sites of defect are thermo-mechanically activated by operation of external mechanical stress, giving rise to the localized basic movements of few atoms, preferentially oriented along the maximum shear plane. The activation and growth of SMDs correspond to the anelastic deformation. The elastic energy stored in the surface surrounding the SMDs is able to induce constriction when the stress is released. Finally, when expanding, SMDs eventually percolate and the resultant deformation is irreversible.

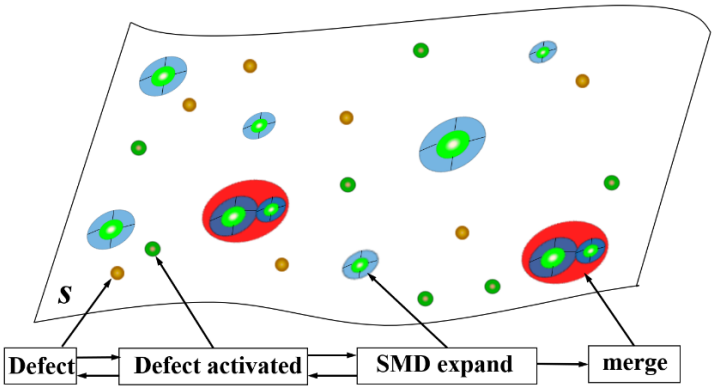

Fig. 1 Scheme of the microstructural arrangements for a glassy solid.

To quantitatively compare the macroscopic anelastic and plastic deformation, we must consider the kinetic aspects of activation and annihilation of the deformation elements. Based on the former description of STZs and SMDs, the following two processes can be distinguished: (i) the formation of SMDs with a characteristic time τ_1 and (ii) the annihilation of SMDs with characteristic time τ_2. After annihilation of SMDs, the initial sites of defect might be activated to generate other SMDs. With the preceding definition, we may describe the kinetic behavior of activation and annihilation of SMDs by the equation (Perez, 1998):

$$\frac{dn(t_{\exp})}{dt} = -\frac{n(t_{\exp}) - n(\infty)}{\tau_1} + \frac{n(0) - n(t_{\exp})}{\tau_2} \tag{12}$$

where $n(t_{\exp})$ is the number of the non-activated SMDs per volume. The anelastic deformation results not only from the formation of SMDs but also from the expansion of these SMDs. Referring to the analysis of the hierarchical correlation effects given by Eq. (7), the anelastic deformation process spreads on a time scale between τ_β and $\tau_{\max}$ with $\tau_2 \approx \tau_{\max}$ since the end of anelasticity is imposed by the annihilation of the SMD. Therefore, Eq. (12) can be written as:

$$\frac{dn(t_{\exp})}{dt} = -\frac{n(t_{\exp}) - n(\infty)}{\tau_1(t)} + \frac{n(0) - n(t_{\exp})}{\tau_{\max}} \tag{13}$$

In the following, we split our discussion in to two limiting situations in order to solve this differential equation.

3.3.1 Anelastic deformation

At short time ($\tau_\beta < t_{\exp} < \tau_{\max}$), the last term describing the annihilation of SMDs in Eq. (13) can be neglected, and this equation reduces to:

$$\frac{dn(t_{\exp})}{dt} = -\frac{n(t_{\exp}) - n(\infty)}{\tau_1(t_{\exp})} \tag{14}$$

Its integration leads to:

$$n(t_{\exp}) = n(\infty) + (n(0) - n(\infty)) \cdot \exp\left[-\left(\frac{t_{\exp}}{\chi^{1/\chi}\tau_{\max}}\right)^{\chi}\right] \tag{15}$$

Therefore, the formation of a SMD and its expansion gives rise to a local shear equal to $\Delta\varepsilon_{\text{an}}$ in a volume v_0 of the matter. This results in a macroscopic deformation equal to $\Delta\varepsilon_{\text{an}} * v_0/V_{\text{tot}}$ in the volume V_{tot} of matter. By considering the nucleation rate of the SMDs in the volume V_{tot}, the rate of anelastic deformation is written as:

$$\frac{d\varepsilon_{\text{an}}}{dt_{\exp}} = \frac{\Delta\varepsilon_{\text{an}} \cdot v_0}{V_{\text{tot}}} \cdot \frac{n(t_{\exp}) - n(\infty)}{\tau_1(t_{\exp})} \cdot V_{\text{tot}} \tag{16}$$

the solution of which is:

$$\varepsilon_{\text{an}} = A_{\text{an}} \cdot \sigma \cdot \left\{1 - \exp\left[-\left(\frac{t_{\exp}}{\tau_{\text{an}}}\right)^{\chi}\right]\right\} \tag{17.a}$$

with

$$\tau_{\text{an}} = \chi^{1/\chi}\tau_{\max} \tag{17.b}$$

where A_{an} is regarded as the intensity of the anelastic process.

3.3.2 Plastic deformation

At longer time, $n(t)$ tends towards $n(\infty)$ and the first term of the right hand of Eq. (13) vanishes, hence we have:

$$\frac{dn(t_{\exp})}{dt_{\exp}} = \frac{n(0) - n(\infty)}{\tau_{\max}} \tag{18}$$

The macroscopic plastic deformation resulted from the annihilation of a SMD should be greater than but not very different from $\Delta\varepsilon_{\text{an}} \cdot v_0/V_{\text{tot}}$. If we are generous and accept that the two quantities are equivalent, the plastic deformation can be written as:

$$\varepsilon_{\text{vp}} = A_{\text{vp}} \cdot \sigma \cdot \frac{t_{\exp}}{\tau_{\max}} \tag{19}$$

where the intensity A_{vp} of the plastic component is about A_{an}.

3.3.3 β relaxation

It is widely accepted that the glassy matter, irrespectively of its particular nature, exhibits two relaxation processes, i.e., α and β. Previous studies (Debenedetti and Stillinger, 2001; Johari, 1973; Qiao et al., 2017) have shown that there is only one relaxation behavior at a high temperature ($T > 1.2T_g$), and the viscosity and coefficient of diffusion obey the Stokes-Einstein equation. In the moderately supercooled regime, the single relaxation behavior splits into β and α relaxations. The former could be described by the Arrhenius law, and the latter exhibits the Vogel-Fulcher-Tammann (VFT) equation form and becomes extremely slow at T_g (Debenedetti and Stillinger, 2001; Geirhos et al., 2018; Luo et al., 2017).

The anelastic and plastic components of deformation are mainly associated with the primary relaxation (α relaxation). While the β relaxation is associated with local motions of a limited number of atoms in metallic glass. Referring to the derivation process of anelastic strain, the deformation related to β relaxation (rearrangement of a certain number atoms) can be calculated by the following equation:

$$\varepsilon_\beta = A_\beta \sigma \left[1 - \exp\left(-\frac{t_{\exp}}{\tau_\beta}\right)\right] \tag{20}$$

3.3.4 The total deformation

A complete expression for the total deformation (ε) is thus given by the sum of elastic deformation (ε_{el}), deformation linked to β relaxation (ε_β), anelastic deformation (ε_{an}) and plastic deformation (ε_{vp}). From the expressions (17), (19) and (20), we may express the total deformation in the form of compliance, $J_{\text{tot}}(t) = \varepsilon/\sigma$,

$$J_{\text{tot}}(t_{\exp}) = J_{\text{el}} + J_\beta + J_{\text{an}} + J_{\text{vp}} =$$

$$\frac{1}{E_{\text{el}}} + A_\beta \left[1 - \exp\left(-\frac{t_{\exp}}{\tau_\beta}\right)\right] + A_{\text{an}} \left\{1 - \exp\left[-\left(\frac{t_{\exp}}{\tau_{\text{an}}}\right)^\chi\right]\right\} + A_{\text{vp}} \frac{t_{\exp}}{\tau_{\max}} \tag{21}$$

where E_{el} is storage modulus at ambient temperature.

The calculations of the above equation depend on an important parameter – the correlation parameter χ – which increases with disorder of system and therefore also with the concentration of defect C_{d}. χ is assumed to be linearly related to C_{d} when temperature is slightly higher than T_g. On the other hand, χ is a constant when metallic glass is in an iso-configurational state at $T < T_g$. In addition, we should also ask whether χ remains constant during deformation, and if not, how it evolves. Due to the fact that the final configuration of defects after annihilation of SMDs should be no different from the initial defect site, the correlation parameter χ is independent of plastic deformation. It should be noted that in the case of amorphous polymer, the

elongation of chains will impose the correlation effects at longer distance (i.e. a decrease in χ) (Rinaldi et al., 2011). In addition, by considering the increase of disorder when the anelastic component increases, the following simple evolution laws for the correlation parameter are added

$$\chi(T) = \chi(T_g) \qquad \text{for } T < T_g \tag{22.a}$$

$$\chi(T) = \chi(T_g) + a_1(T - T_g) \qquad \text{for } T > T_g \tag{22.b}$$

$$\chi(T, \varepsilon) = \chi(T) + a_2 \varepsilon_{an} \tag{22.c}$$

where a_1 is an adjustable parameter and it is material specific. $\chi(T)$ in Eq. (22.c) is the initial value of the correlation parameter at the beginning of test and ε_{an} is the anelastic contribution to the total deformation. In the following experimental part of this study, we will give the evolution curves of χ with both temperature and strain. Frankly, this is a fairly simplified description of the evolution of correlation factor with deformation. This description is applicable when the defect concentration is not far from equilibrium. In fact, a more accurate description should consider both deformation-induced disordering (increase of χ) and diffusion-controlled reordering (decrease of χ)

3.5 Linear viscoelastic regime

The linear viscoelastic behavior is investigated by DMA, i.e., the evolution of complex shear (or Young's) modulus $G^*(or\ E^*)$ as a function of temperature T and the angular frequency ω, we should translate Eq. (21) from time domain to frequency domain with the help of classic time-frequency analysis tool. Firstly, we develop Eq. (21) by expanding the anelastic term to Taylor series and keeping just the first term to approach the linear response. Therefore, the Laplace-Carson transform of Eq. (21) directly gives access to the expression of the frequency response of the material

$$J^*(i\omega) = \frac{1}{E_{\text{el}}} + A_\beta \frac{1}{1 + i\omega\tau_\beta} + A_{\text{an}} \frac{1}{(i\omega\tau_{\text{an}})^\chi} + A_{\text{vp}} \frac{1}{i\omega\tau_{\max}} \tag{23}$$

where ω is the angular frequency ($\omega = 2\pi f$ with f the driving frequency of DMA test). It should be noted the complex modulus $E^*(i\omega)$ is the inverse of $J^*(i\omega)$ expression. Therefore, the storage modulus E' and loss modulus E'' can be simply deduced from the real part J' and imaginary part J'' of $J^*(i\omega)$.

3.6 Spectrum of characteristic times

Due to the disordered arrangement of atoms in MGs, there is no reason to take a single value of U_β in Eq. (8) (Egami, 2011; Luckabauer et al., 2019; Yang et al., 2012b). Many works have shown that there is an activation energy distribution with a certain shape such as normal or Gumbel ones (Bruns et al., 2021; Rinaldi et al., 2011; Shang et al., 2019). In view of the fact that the distribution of characteristic times is

asymmetric, i.e. the distribution extends much more towards the side of short times than that of long times, it is adequate to use a Gumbel distribution (Bertin, 2005; Rinaldi et al., 2011):

$$W_\beta^i = \frac{\exp\left\{B\ln\left(\frac{\tau_{\beta i}}{\langle\tau_\beta\rangle}\right) - \exp\left[B\ln\left(\frac{\tau_{\beta i}}{\langle\tau_\beta\rangle}\right)\right]\right\}}{\sum_i \exp\left\{B\ln\left(\frac{\tau_{\beta i}}{\langle\tau_\beta\rangle}\right) - \exp\left[B\ln\left(\frac{\tau_{\beta i}}{\langle\tau_\beta\rangle}\right)\right]\right\}} \tag{24}$$

where B is the distribution width and $\langle\tau_\beta\rangle$ the most probable value of $\tau_{\beta i}$. W_β^i represents the statistical weight of each characteristic time $\tau_{\beta i}$.

As a consequence, we finally reach the constitutive relation for mechanical response of MG:

$$J_{\text{tot}}(t_{\text{exp}}) = \frac{1}{E_{\text{el}}} + A_\beta \sum_i W_\beta^i \left[1 - \exp\left(-\frac{t_{\text{exp}}}{\tau_{\beta i}}\right)\right] \quad + +A_{\text{an}}\left\{1 - \exp\left[-\left(\frac{t_{\text{exp}}}{\tau_{\text{an}}}\right)^\chi\right]\right\}$$

$$+ A_{\text{vp}}\frac{t_{\text{exp}}}{\tau_{\text{max}}} \tag{25.a}$$

$$J^*(i\omega) = \frac{1}{E_{\text{el}}} + A_\beta \sum_i W_\beta^i \frac{1}{1 + i\omega\tau_{\beta i}} + A_{an}\frac{1}{(i\omega\tau_{\text{an}})^\chi} + A_{vp}\frac{1}{i\omega\tau_{\text{max}}} \tag{25.b}$$

It is thus possible to calculate the stress-strain (or strain-time) curves of conventional mechanical tests (tension and creep) form Eq. (25.a), so one can verify applicability of the current theory under the condition of large deformation. Eq. (25.b), the Laplace-Carson transform of Eq. (25.a), directly gives the expression of complex compliance to describe dynamic mechanical behavior (periodic stress or strain), which is effective to study the relaxation behavior of metallic glass. Therefore, two kinds of experiments, dynamic mechanical analysis experiment (small strain) and tensile and creep tests (large strain), are carried out in the current work.

For clarity, a graphical illustration of the Gumbel distribution is given with different B parameters is given in Fig. 2.

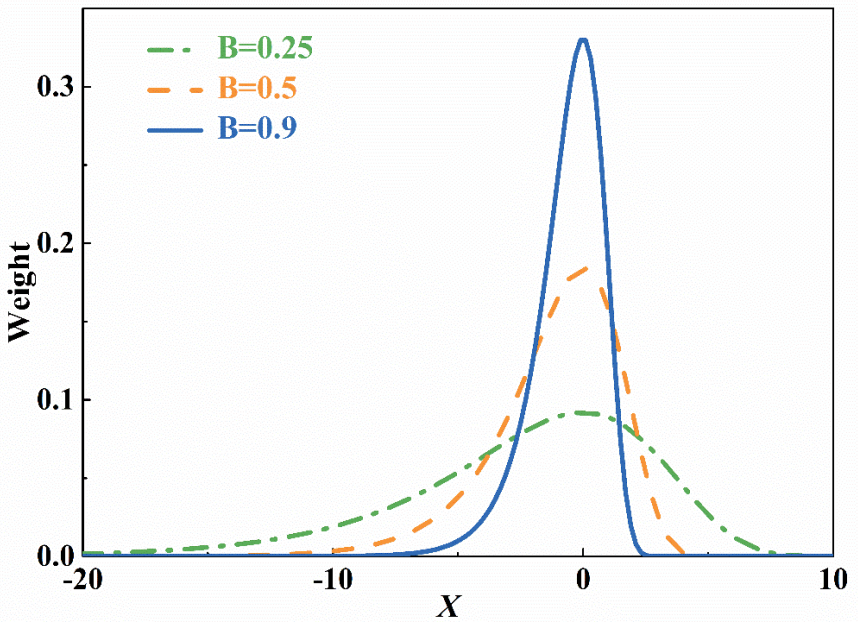

Fig. 2 Gumbel distribution with different width parameter B.

4. Model parameters

From the DMA linear viscoelastic experiments and the finite strain tests described in Section 2, the material parameters of the theoretical model can be calculated and evaluated.

4.1 Elastic process

J_{el} is the initial elastic compliance, taken as the inverse of the unrelaxed storage modulus E_{u_β} ($J_{\mathrm{el}} = 1/E_{\mathrm{el}} = 1/E_{\mathrm{u}\_\beta}$).

4.2 β relaxation process

The intensity of β relaxation A_β, apparent activation energy of β relaxation U_β and the pre-exponential time $\tau_{\beta 0}$ can be determined from the characterization of the β relaxation process in DMA linear viscoelastic experiments described in section 2.2. The intensity of β relaxation A_β can be calculated by $1/E_{\mathrm{r}\_\beta} - 1/E_{\mathrm{u}\_\beta}$. The unrelaxed elastic modulus E_{u_β} and the relaxed elastic modulus E_{r_β} are directly obtained from the value of the $E'(T)$ curve below and above the β relaxation temperature region, respectively. The relaxation time τ_β at the peak temperature of β relaxation is obtained as $\tau_\beta \approx 1/2\pi f$ (f is the driving frequency) from the isochronal measurements. $\tau_{\beta 0}$ and U_β can be determined by fitting the relationship between relaxation time τ_β and temperature T with Eq. (8), as shown in Fig. 3(c). In addition, the distribution width parameter B of β relaxation is determined from the fit of the loss modulus $E''(T)$ curve in the β relaxation domain, which will be discussed in Section 5.

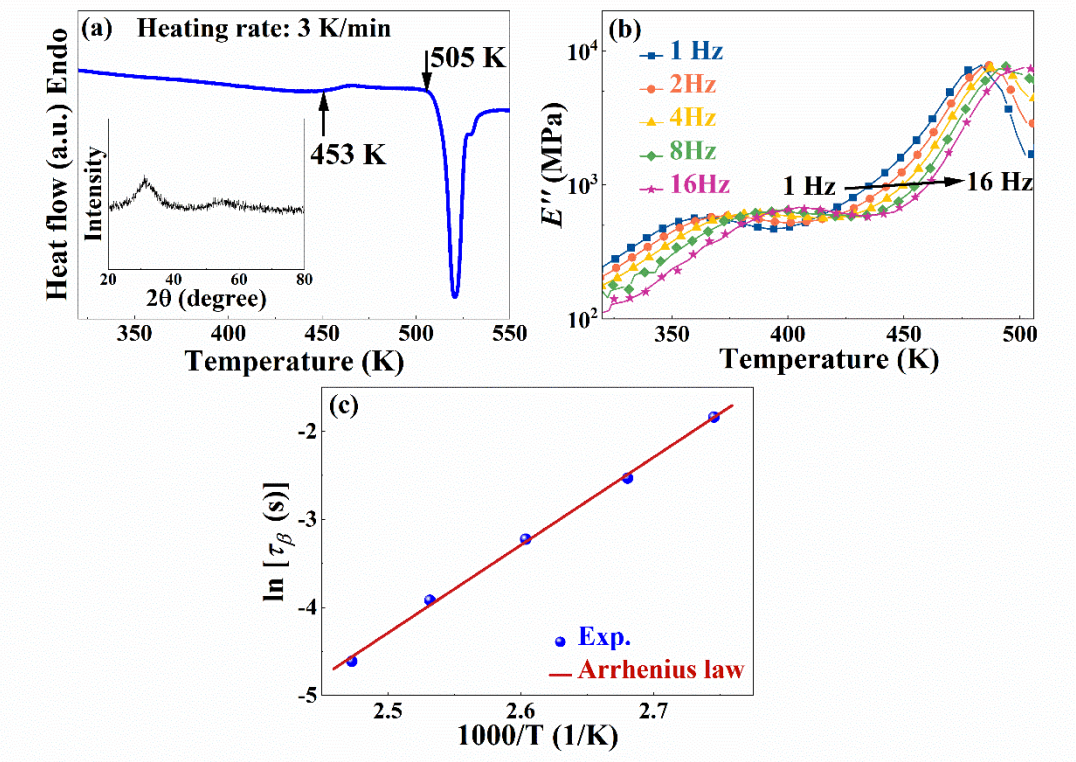

Fig. 3 (a) DSC curve of $La_{60}Ni_{15}Al_{25}$ metallic glass with a heating rate of 3 K/min. Inset is the XRD pattern. (b)Variation of the loss modulus as a function of temperature with different driving frequencies (1-2-4-8-16 Hz) at a given heating rate of 3 K min^{-1}; (c) Correlation between the characteristic time τ_β and the peak value temperature of the β relaxation. The solid line is fitted by the Arrhenius law.

4.3 α relaxation process

The correlation parameter $\chi(T)$, the intensity A_{an} of the anelastic process, the intensity A_{vp} ($A_{\mathrm{vp}} \approx A_{\mathrm{an}}$) of the viscoplastic process and the scale parameter t_0 are devoted to the description of the main α relaxation.

The correlation parameter as a function of temperature described by Eq. (22) should be recalled here. When $T < T_g$, $\chi(T)$ remains constant. On the contrary, $\chi(T)$ almost linearly increases with increasing temperature above T_g. In the literature it is suggested that the internal friction $\tan\delta$ may be described by the equation (Gadaud and Pautrot, 2003; Wang et al., 2005):

$$\tan\delta = (\omega\tau_{\max})^{-\chi} \tag{26}$$

By putting the value of $\tau_{\max}$ in this expression, Eq. (26) can be written in the form:

$$\ln(\tan\delta) = -\frac{U_\beta}{kT} - \chi\ln(\omega) - \chi\ln\left[t_0\left(\frac{\tau_{\beta 0}}{t_0}\right)^{\frac{1}{\chi}}\right] + \ln K \tag{27}$$

where K is a constant. In this case, a double logarithmic plot of $\tan\delta$ versus frequency

at a fixed temperature will give the evolution of χ with temperature.

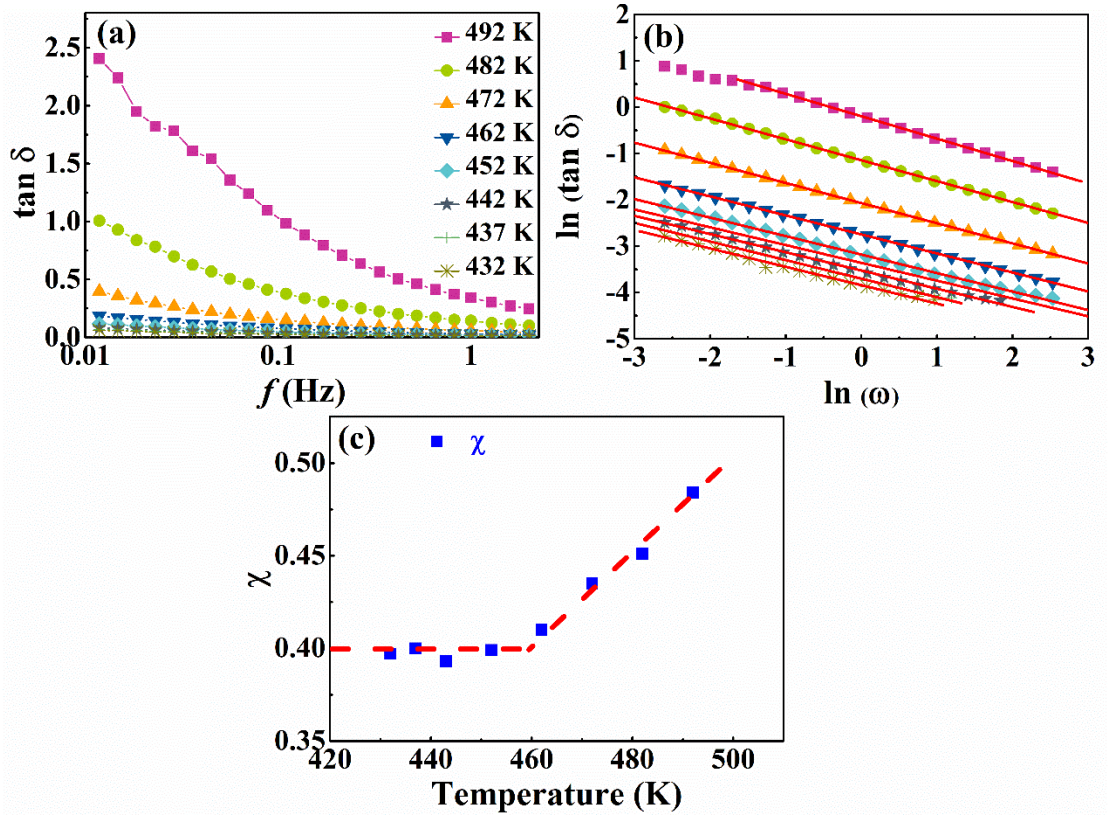

Fig.4 (a) Internal friction of the $La_{60}Ni_{15}Al_{25}$ metallic glass as a function of frequency at different temperatures; (b) Effect of driving frequency on logarithm of internal friction $\tan\delta$ at different temperatures. The solid lines are fitted by Eq. (27); (c) Evolution of the correlation parameter χ with temperature.

As can be seen in Fig. 4(a), isothermal internal friction spectrum is measured over a broad temperature region with varying driving frequency. Fig. 4(b) shows the variations of $\ln(\tan\delta)$ versus $\ln(\omega)$ at different temperatures and the experimental results could be well described by the Eq. (27). Fig. 4(c) shows the variation of the correlation parameter χ with temperature for the $La_{60}Ni_{15}Al_{25}$ metallic glass. It has been shown that χ ranges from 0.38 to 0.4 for typical MGs in our previous work (Qiao and Pelletier, 2014; Qiao et al., 2016b).

Scale parameter t_0 is related to the shift between the two relaxations: the smaller the t_0, the closer the α and β relaxation processes. Therefore, a value of 6×10^{-7} s for t_0 is found to give the best fit of the isochronal curve. Finally, A_{an}, the intensity of the anelastic process, can be adjusted so that the calculated and experimental curves for the G'' peak obtained at a given frequency coincide. Finally, there are only two left parameters (σ_0 and a_2) that cannot be obtained from the linear DMA experiments, which are adjusted to match the stress-strain curve at 430 K. Table 1 lists the set of parameters, together with their physical significances, and the values determined for the $La_{60}Ni_{15}Al_{25}$ metallic glass.

Table 1 Parameters of the current model for $La_{60}Ni_{15}Al_{25}$ metallic glass.

Parameter	Value	Description
E_{u_β} (MPa)	3.3×10^4	Storage elastic modulus before the β relaxation
E_{r_β} (MPa)	3.06×10^4	Relaxed Storage elastic modulus after the β relaxation
U_β (kJ/mol)	83.12	Apparent activation energy of the β relaxation process
$\tau_{\beta 0}$ (s)	1.86×10^{-13}	Pre-exponential factor the β relaxation
A_{an} (A_{vp}) (MPa^{-1})	1.5×10^{-5}	Intensity of anelastic and viscoplastic processes
$\chi(T_g)$	0.4	Correlation parameter below the glass transition temperature T_g
a_1	0.00231	Temperature contribution to the correlation parameter above T_g
t_0 (s)	6×10^{-7}	Scaling parameter related to the shift between α and β relaxations
σ_1 (MPa)	28000	A parameter related to the effect of stress to activation of the β process
a_2	1.8	Anelastic contribution to the correlation parameter

5. Results and discussion

The physical model of hierarchically correlated movements described in Section 3 is implemented for numerical calculations of the small-strain linear viscoelastic dynamic mechanical response and the large-strain plastic deformation behavior. The model parameters and methods for determining the parameters for $La_{60}Ni_{15}Al_{25}$ metallic glass have been described in Section 4.

5.1 Linear regime: DMA

5.1.1 Temperature dependence at a given frequency

DMA temperature scanning techniques can be used to investigate the relaxation process and the evolution of dynamic mechanical properties with temperature in metallic glasses. Under a heating rate of 3K min^{-1}, isochronal DMA experiments for $La_{60}Ni_{15}Al_{25}$ bulk metallic glass were conducted at fixed driving frequency of 1 Hz from room temperature to 550 K. Fig. 5 shows the variation of the storage modulus E' and the loss modulus E'' as a function of temperature. The value of storage modulus is around 33 GPa for this metallic glass at ambient temperature. Similar to the phenomenon observed in other metallic glasses, three typical temperature regions can be distinguished from Fig. 5: (i) In the temperature region from 300 K to 430 K (β relaxation process), E' drops slightly and E'' shows a distinct peak around 360 K. It should be noted that only few families of metallic glasses show a well resolved β relaxation based on the DMA measurements. For most metallic glasses, only a

"shoulder" or "excess wing" on the low temperature side of the α relaxation spectra can be observed. Recent investigations demonstrated that the β relaxation is of importance for understanding some key issues in metallic glasses, such as diffusion (Ngai et al., 2017), physical aging (Yu et al., 2014) and deformation mechanisms (Lei et al., 2020; Wang et al., 2017; Zhang et al., 2019); (ii) In the temperature range of 430 K-500 K (main α relaxation), E' decreases sharply while the loss modulus E'' increases with temperature. E'' shows a maximum value around 480 K. The main α relaxation detected around T_g is associated to the dynamic glass transition phenomenon, which is originated by the cooperative movements of the atoms or molecules of glassy materials, including glassy polymers, oxide glasses and metallic glasses; (iii) When the temperature surpasses 500 K, both E' and E'' increase as temperature increases due to the onset of crystallization.

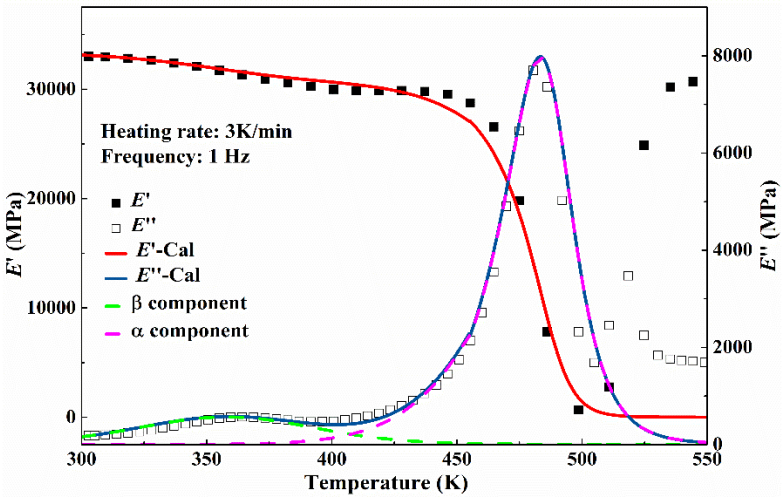

Fig. 5 Symbols: Isochronal curves of $La_{60}Ni_{15}Al_{25}$ bulk metallic glass between 300 and 550 K (f = 1 Hz) measured at a heating rate of 3 K min^{-1}. Solid lines: calculated curves using Eq. (25b). The dashed lines give the individual contributions of the α and β relaxations.

The solid lines in Fig. 5 show the evolution curves of E' and E'' with temperature calculated by Eq. (25b). As shown by the comparison with experimental results, the model is able to capture both the α and β relaxation processes reproducing the $E''(T)$ curve and the sharp decrease of E' in the glass transition region. However, it should be noted that the calculated curves, in the two temperature ranges of $400\ \mathrm{K} < T < 450\ \mathrm{K}$ and $520\ \mathrm{K} < T$, cannot describe well the experimental data. The former is due to possible structural relaxation, which is not taken into account as we assume a constant correlation parameter χ below T_g, and the latter is attributed to the occurrence of crystallization.

It should be noted that a fast β' relaxation process with a well separated E'' peak have been investigated in the temperature range $0.25 - 0.58\ T_g$ for all the MGs in addition to α and β relaxation processes (Wang et al., 2017; Zhao et al., 2016). The fast β' relaxation possesses a fairly low activation energy, only about half of that of the β

relaxation process. On the other hand, not all β relaxation in metallic glasses can be observed as a distinctive and complete E'' peak. By comparison, the β relaxation emerges in the form of either a shoulder (Pd-, Mg-based MGs) or even an excess wing (Zr-, Cu-based MGs). Therefore, to enable the model to be applicable to other MGs, the theoretical calculation of temperature spectrum including the fast β' relaxation process is given, by considering the appropriate values of activation energy and distribution width, as shown in Fig. 6(a). Further, we also give the calculated curves of different forms of β relaxations by selecting appropriate scaling parameter t_0 in Fig. 6 (b).

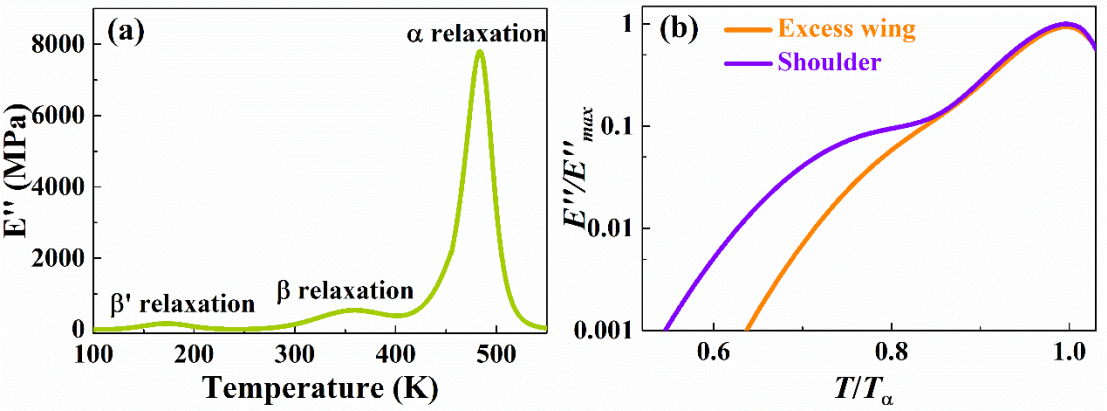

Fig. 6 Theoretical calculations for the DMA isochronal curves. (a) Different relaxation behaviors including the distinctive fast β' relaxation process; (b) Different forms ('excess wing' and 'shoulder') of β relaxation.

5.1.2 Effect of testing frequency

To investigate the effect of driving frequency on the dynamic mechanical behavior, a series of isothermal measurements were conducted over a large temperature range (322 K–492 K; temperature interval 10 K) with varying test frequency (0.01–2 Hz). Based on the time-temperature superposition (TTS) principle, the resultant master curve (as shown in Fig. 7) covers a frequency range much greater than that of the original test data. The red solid line is the best fit of the master curve of the loss modulus according to Eq (25b), and it is shown to accurately describes the isothermal spectra of α and β relaxation processes.

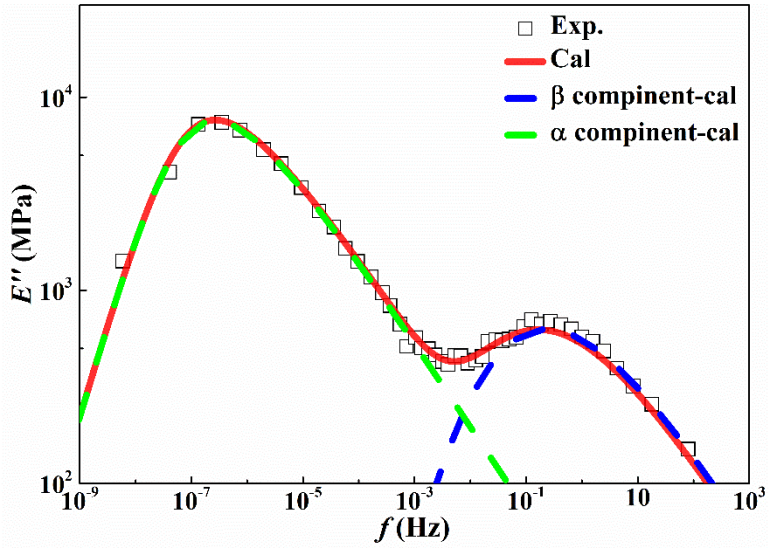

606

607 **Fig. 7** Symbols: Master curve of the loss modulus E'' for $La_{60}Ni_{15}Al_{25}$ metallic glass.
608 Red solid line: calculated curve. The dashed lines denote individual contributions to the
609 α and β relaxations, respectively.

610 The limitation of validity of a master curve for analysis based on TTS needs to be
611 considered. In fact, the TTS is not valid for the whole temperature range. That is
612 because it assumes that the shape of the spectrum at each temperature is the same but
613 shifted in the frequency or time scales, which is obviously incorrect. Therefore, the TTS
614 is generally used to show different relaxation processes, rather than to study the
615 dynamic characteristics of α or β relaxation processes. Consequently, the scaling
616 parameter t_0 in the model, which is related to the shift between α and β relaxations, is
617 adjusted to obtain a better agreement with the experimental data.

618 *5.1.3 Evolution of characteristic times*

619 One of the intriguing questions in the study of the relaxation behavior of metallic
620 glasses is how to separate the contribution of α and β relaxation in the master curve,
621 which has been discussed above. As shown in Fig. 8, the change of relaxation time for
622 the α and β processes as a function temperature can be described based on the current
623 model, which is in good agreement with the experimental data (solid symbols). It can
624 be noted that the variation of τ_β with temperature is consistent with the Arrhenius
625 equation over the whole temperature (purple solid line). For the characteristic time $\tau_{\max}$,
626 it obeys the VFT equation in the metastable equilibrium ($T > T_g$). As decreasing
627 temperature, $\tau_{\max}$ increases very rapidly. The increase corresponds not only to the
628 decrease in thermal activation but also to the increase of cohesion (decrease of specific
629 volume and configurational entropy). The latter is the basis of the VFT law.
630 Furthermore, the VFT behavior followed at high temperatures changes to an Arrhenius-
631 like response below T_g rather than to the vertical asymptote as sometimes described. At
632 $T < T_g$, the system is in an iso-configurational state and the correlation parameter χ is
633 constant. Therefore, an Arrhenius law is observed for both $\tau_{\max}$ and τ_β. An analysis of

hierarchically correlated movements might well explain the surprising transition behavior of characteristic time $\tau_{\max}$ from one side to the other side of T_g. In fact, the understanding of characteristic time and atomic mobility is of importance to physical aging and mechanical properties of metallic glasses (Casalini and Roland, 2009; Luo et al., 2017; Qiao et al., 2016a; Yu et al., 2017).

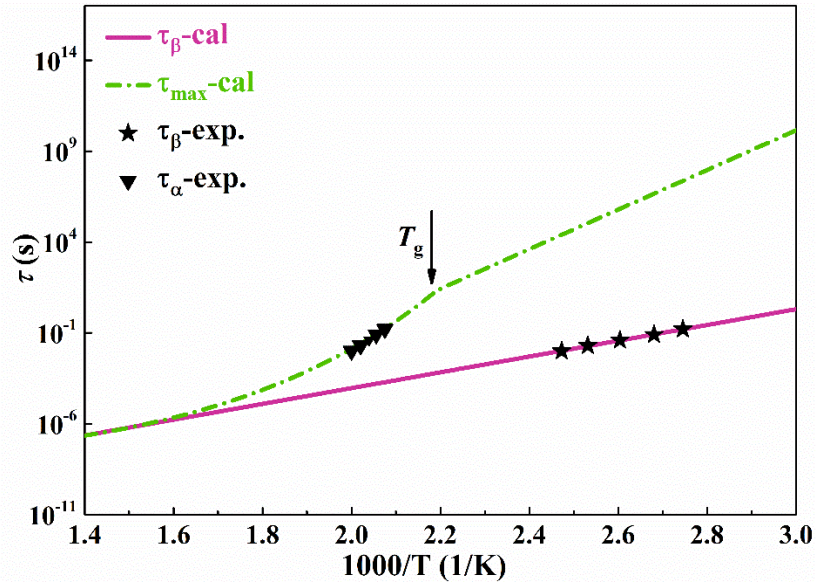

Fig. 8 Variation of the characteristic times for α and β relaxations, respectively, as a function of temperature. Black symbols stand for the experimental values of τ_α and τ_β determined by the relation $\omega\tau = 1$ at the peak of the loss modulus; Purple solid line represents the variation of τ_β with temperature calculated from Arrhenius law; Green dashed line denotes the variation of $\tau_{\max}$ with temperature according to the theoretical model proposed in this work.

According to the current knowledge, two main kinetic processes are related to relaxation in glassy state, i.e., the fast β Johari-Goldstein (JG) relaxation and the slow α relaxation described in Fig. 8. It may have explained the two-step stress relaxation phenomenon found in recent works (Bruns et al., 2021; Luo et al., 2017; Soriano et al., 2021). They found a surprising gradual change of stress relaxation process from a single-step to a two-step decay upon cooling. The faster relaxation process is likely due to the microscopic dynamics dominated by the anomalous stress, and the slower one is related to diffusive motion at larger scales with a broad distribution of relaxation times. The fast decay observed by them and the fast JG relaxation process were incompatible on both the time scale and the activation energy, which we believe may be due to three reasons as explained in the following. Primarily, one reason is the limit of the time scale of the experimental observation ($1 \sim 10^5$ s), which leads to that a part of stress relaxation caused by fast β relaxation is difficult to be detected because its response time is too short; Secondly, the plastic deformation caused by the coalescence of the neighboring SMDs may be companied by the recovery of isolated SMDs; Thirdly, the deformation unit will lose its independence, not only due to the coalescence of SMDs, but also due

to the diffusion of defects between two neighboring SMDs. Such a mechanism is well-known in the kinetics of dislocation. Fig. 9 shows the stress relaxation profiles calculated by Eq. (25a) at different temperatures. The stress $\sigma(t)$ have been normalized by the initial stress σ_0. As observed in the figure, the stress decreases by a single-step fashion near T_g. However, as the temperature decreases, the stress relaxation is gradually decoupled into well-defined two steps. It should be noted that the two-step stress relaxation behavior of metallic glasses in non-equilibrium state is closely related to the state of glass and provides a new clue to understand the nonelastic deformation, as well as dynamic heterogeneity as expected in metallic glasses. Therefore, the consistency between experiment and theoretical calculation deserves further studies.

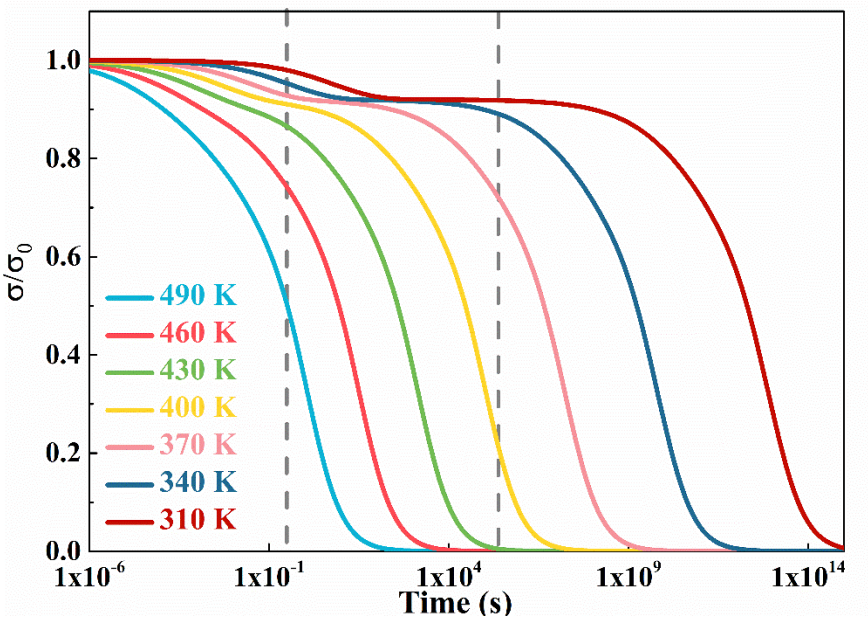

Fig. 9 Stress relaxation curves from 310 to 490 K calculated by Eq. (25a). The magnitude of stress σ has been normalized by the initial value σ_0.

5.2 Non-linear regime: Finite deformation tests

In section 5.1, a good description for the dynamic mechanical relaxation phenomenon with small amplitude oscillatory loading conditions was obtained. With the confidence that the previous validation of the model brings to us, another important goal is to apply the model to the finite strain experiments of large deformation.

5.2.1 Uniaxial tensile tests at a given strain rate

The deformation behavior of metallic glasses is very sensitive to temperature. At low temperature, the deformation is not homogeneous, and takes place locally with quite higher degree than the rest part. However, with the increase of temperature ($T > 0.8\,T_g$), especially in the supercooled liquid region, the nonelastic deformation is rather homogeneous in the entire solid, which not only has important application value in molding, but also is of significance for understanding microstructural evolution of

nonelastic deformation of metallic glasses, so it has attracted extensive attention.

Previous reports have emphasized on the effect of temperature, strain rate, stress, physical aging and hydrostatic pressure on macroscopic deformation (Schuh et al., 2007; Shi and Falk, 2007). In order to determine the contribution of elastic, anelastic and plastic deformation components and the evolution law of each component in the deformation process, several samples must be unloaded after deformation up to different strain levels under uniaxial tension. The recovered part embeds the elastic (instantly reversible) and anelastic (reversible but delayed) contributions, whereas the irreversible permanent deformation is called plastic, as shown in Fig. 10(a). In Fig. 10(b), it is shown that the elastic and anelastic parts onset at the beginning of the deformation and tend to be stable in the stage of steady-state flow. The plastic deformation occurs latter, but increases rapidly at a stable growth rate. In the current work, the theoretical predictions based on the hierarchically correlated movements of the evolution of the total stress, elastic, anelastic and plastic contributions during the finite tensile test at the given strain rate of 3×10^{-4} s^{-1} have been confronted to the experimental results. In spite of the success of the model, the evolution of deformation units (SMDs, STZs, …) and their potential activation sites (QPDs, free volume, …), in the process of competition between stress induced production of defects and thermal annihilation, should be clarified. It is important to note that defect is a feature of the glass structure and can be identified based on the fluctuations of density, enthalpy and entropy. However, an SMD/STZ is not a structural defect and is defined by its transience, that is, it cannot be identified at a single instant in time (Schuh et al., 2007).

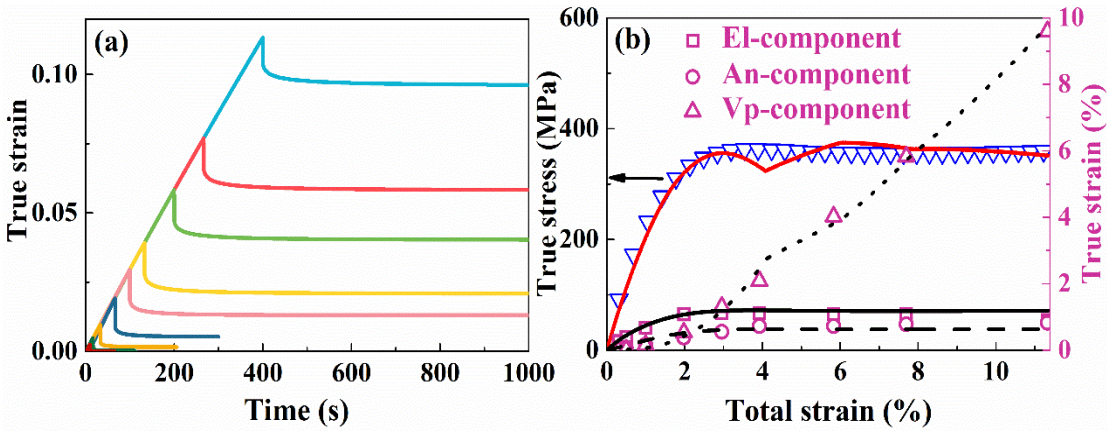

Fig. 10 (a) Experimental true strain-time curve for $La_{60}Ni_{15}Al_{25}$ metallic glass in a set of uniaxial tensile and subsequent recovery measurements. (b) Evolution of the elastic, anelastic and viscoplastic strains during deformation. The test temperature is 430 K and the strain rate is 3×10^{-4} s^{-1}. The peak stress is about 370 MPa. The elastic modulus is calculated as 29.8 GPa from the initial slope of stress-strain curve. Symbols: experimental data; Curves: theoretical calculations.

5.2.2 Creep and recovery

The creep recovery experiments were carried out at a given temperature (i.e., 430 K) with different uniaxial tensile stresses (25 and 50 MPa, respectively). The creep time is 330 s. As shown in Fig. 11, it is interesting to point out that the creep behavior of the model alloy exhibits two states: the transient state and the steady-state stage. Indeed, the two-stage phenomenon occurs at low stress levels. In contrast, at high-stress levels, three stages should appear in the creep process: following the steady-state stage is the tertiary stage where the strain rate starts surging, as reported in the previous literature (Zhu et al., 2021). It should be pointed out that the third stage of creep behavior under high is not shown in the current work, because the inhomogeneous deformation (shear localization) reflected in the third stage cannot be described by the current version of hierarchical correlation theory. In this case, the separation of flow into shear bands and remaining matrix should be consider, which lies beyond the scope of the current investigation. The origin of the two distinct cases lies in the fact that the chemical potential under thermo-mechanical coupling is a function of defect concentration and stress state. At low stress levels, the chemical potential is dominated by the thermal effect, which tends to smooth out the heterogeneity of the metallic glass. In comparison, at high stress levels, the stress concentration dominates that increasing of the heterogeneity of metallic glasses (Zhu et al., 2021). Three deformation components can be derived from the recovery curves. According to the preceding analysis, the anelastic and plastic contributions are associated with the expansion and coalescence of deformation units, respectively. In fact, the evolution of anelastic strain can be studied by the small-deformation experiments at low temperature. Since the values of deformation was very small, almost comparable to those of elastic deformation, SMDs accommodating anelastic deformation are isolated and did not interact with each other (Atzmon and Ju, 2014; Ju et al., 2011; Lei et al., 2020).

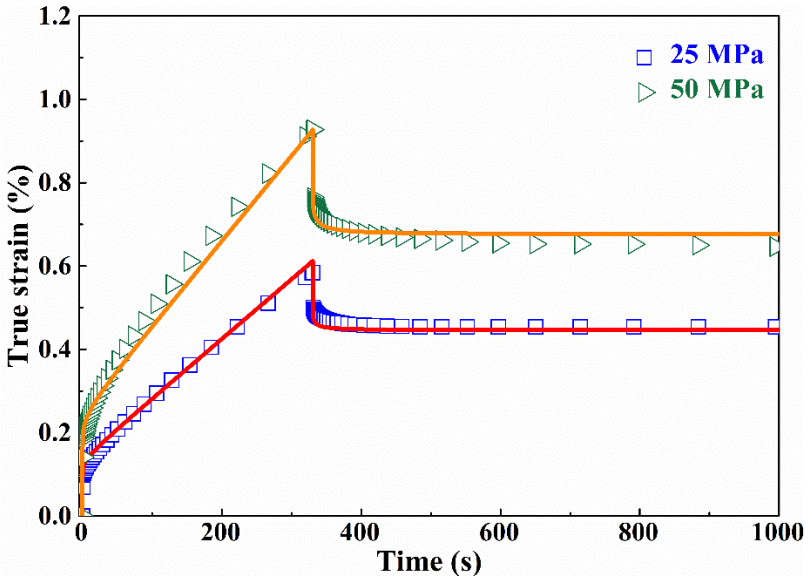

Fig. 11 Comparison between theoretical calculations (lines) and experiments (symbols) for creep at 430 K.

As shown by the comparison with experimental results in Fig. 11, the model is able to capture the evolution of strain with time during creep and recovery. In spite of the success of the model, the two aspects of structural evolution and characteristic time need to be further explained in the description of creep and subsequent recovery process. In the case of the microstructural evolution, a single correlation factor is adopted at a given stress for simplicity, which is appropriate for the steady-state flow in the second stage. In fact, if researchers want to describe the micro evolution process more accurately, the unloading experiments after deformation up to different strain should be performed. For the second case, when we remove the stress, the characteristic time for recovery of deformation for the anelasticity should be longer than that of anelasticity during the creep process.

6. Concluding remarks

In this work, a theoretical framework for universal description of the non-elastic deformation of metallic glasses has been presented based on the hierarchically correlated molecular theory and quasi point defect theory. This model describes a much-simplified conceptual scenario of atomic rearrangement. The activation, expansion and coalescence of SMDs are associated with anelastic (reversible) and plastic (permanent) deformation as described in Fig. 1. Hierarchical correlation effects are supposed to occur during atomic movements, i.e., the atomic movements involve more and more atoms and require increasing time to be completed. On the one hand, it is worth to point out that the current research considers the microstructural heterogeneity on the nano-scale. We could not consider the defects from the perspective of the macrostructure, i.e. cavities and notches. It has been proved that these cavities and notches are closely related to the deformation behavior of the glass solids (Chen and Dai, 2016; Pan et al., 2015; Sha et al., 2019; Singh et al., 2013). On the other hand, the current analysis is applicable only in the case of homogeneous deformation. Therefore, plastic instability, necking phenomena and the formation of crazes are not taken into account. In fact, it is obvious that the macroscopic inhomogeneous deformation at lower temperature such as serrated flow, initiation and propagation of shear bands is also affected by the microstructural defects (Chen et al., 2013; Tong et al., 2016; Xie et al., 2019). The mechanical aspects of plastic instability are difficult to quantify. In this case, the description should consider the separation of flow into shear bands covering a fraction f of the volume and remaining matrix covering a fraction (1-f), which lies beyond the scope of the current investigation.

A validation of the current model has been achieved for $La_{60}Ni_{15}Al_{25}$ metallic glass: a good description has been obtained not only for the small-strain linear viscoelastic dynamic mechanical response but also for the large-strain plastic deformation behavior. This provides a bridge between the dynamic mechanical analysis and the conventional mechanical tests, such as creep and uniaxial tensile tests. Actually, the current model

has the potential to be applied to describe various relaxation behaviors in other MGs, such as fast β' relaxation process. In addition, the model also provides a theoretical description for the two-step relaxation phenomenon in deep glassy state, which is helpful to understand the relaxation mechanism and plastic deformation behavior of the generic amorphous materials from a new perspective.

Acknowledgments

This work is supported by the NSFC (Grant No. 51971178) and the Natural Science Basic Research Plan for Distinguished Young Scholars in Shaanxi Province (Grant No. 2021JC-12) E. Pineda acknowledges financial support from MICINN (grant PID2020-112975GB-I00) and Generalitat de Catalunya (grant 2017SGR0042). YJW was financially supported by NSFC (Grant No. 12072344) and the Youth Innovation Promotion Association of the Chinese Academy of Sciences. YY acknowledges financial support from Research Grant Council (RGC), the Hong Kong government through the General Research Fund (GRF) with the grant numbers CityU11200719 and CityU11213118.

References

Afonin, G.V., Mitrofanov, Y.P., Kobelev, N.P., da Silva Pinto, M.W., Wilde, G., Khonik, V.A., 2019. Relationship between the enthalpies of structural relaxation, crystallization and melting in metallic glass-forming systems. Scr. Mater 166, 6-9. https://doi.org/10.1016/j.scriptamat.2019.02.030.

Argon, A., 1979. Plastic deformation in metallic glasses. Acta Metall. 27, 47-58. https://doi.org/10.1016/0001-6160(79)90055-5.

Argon, A.S., Kuo, H.Y., 1979. Plastic flow in a disordered bubble raft (an analog of a metallic glass). Mater. Sci. Eng. 39, 101-109. https://doi.org/10.1016/0025-5416(79)90174-5.

Argon, A.S., Shi, L.T., 1983. Development of visco-plastic deformation in metallic glasses. Acta Metall. 31, 499-507. https://doi.org/10.1016/0001-6160(83)90038-x.

Arsenlis, A., Parks, D.M., 2002. Modeling the evolution of crystallographic dislocation density in crystal plasticity. J. Mech. Phys. Solids 50, 1979-2009. https://doi.org/10.1016/s0022-5096(01)00134-x.

Atzmon, M., Ju, J.D., 2014. Microscopic description of flow defects and relaxation in metallic glasses. Phys. Rev. E 90. https://doi.org/10.1103/PhysRevE.90.042313.

Bertin, E., 2005. Global fluctuations and gumbel statistics. Phys. Rev. Lett. 95, 170601. https://doi.org/10.1103/PhysRevLett.95.170601.

Boyce, M.C., Parks, D.M., Argon, A.S., 1988. Large inelastic deformation of glassy-polymers. 1. Rate dependent constitutive model. Mech. Mater. 7, 15-33. https://doi.org/10.1016/0167-6636(88)90003-8.

Bruns, M., Hassani, M., Varnik, F., Hassanpour, A., Divinski, S., Wilde, G., 2021. Decelerated aging in metallic glasses by low temperature thermal cycling. Physical Review Research 3, 013234. https://doi.org/10.1103/PhysRevResearch.3.013234.

Casalini, R., Roland, C., 2009. Aging of the secondary relaxation to probe structural relaxation in the glassy state. Phys. Rev. Lett. 102, 035701. https://doi.org/10.1103/PhysRevLett.102.035701.

Chen, Y., Dai, L.H., 2016. Nature of crack-tip plastic zone in metallic glasses. Int. J. Plast 77, 54-74. https://doi.org/https://doi.org/10.1016/j.ijplas.2015.10.004.

Chen, Y., Jiang, M.Q., Dai, L.H., 2013. Collective evolution dynamics of multiple shear bands in bulk metallic glasses. Int. J. Plast 50, 18-36. https://doi.org/https://doi.org/10.1016/j.ijplas.2013.03.010.

Cheng, Y.Q., Ma, E., 2011. Atomic-level structure and structure-property relationship in metallic glasses. Prog. Mater. Sci. 56, 379-473. https://doi.org/10.1016/j.pmatsci.2010.12.002.

Cheng, Y.T., Hao, Q., Pelletier, J.M., Pineda, E., Qiao, J.C., 2021a. Modelling and physical analysis of the high-temperature rheological behavior of a metallic glass. Int. J. Plast, 103107. https://doi.org/10.1016/j.ijplas.2021.103107.

Cheng, Y.T., Hao, Q., Qiao, J.C., Crespo, D., Pineda, E., Pelletier, J.M., 2021b. Effect of minor addition on dynamic mechanical relaxation in ZrCu-based metallic glasses. J. Non·Cryst. Solids 553, 120496. https://doi.org/10.1016/j.jnoncrysol.2020.120496.

Debenedetti, P.G., Stillinger, F.H., 2001. Supercooled liquids and the glass transition.

Nature 410, 259-267. https://doi.org/10.1038/35065704.
Egami, T., 1981. Structural relaxation in metallic glasses. Ann. N.Y. Acad. Sci. 371, 238-251. https://doi.org/10.1111/j.1749-6632.1981.tb55664.x.
Egami, T., 2011. Atomic level stresses. Prog. Mater. Sci. 56, 637-653. https://doi.org/10.1016/j.pmatsci.2011.01.004.
Egami, T., Iwashita, T., Dmowski, W., 2013. Mechanical properties of metallic glasses. Metals 3, 77-113. https://doi.org/10.3390/met3010077.
Etienne, S., Cavaille, J.Y., Perez, J., Point, R., Salvia, M., 1982. Automatic system for analysis of micromechanical properties. Rev. Sci. Instrum. 53, 1261-1266. https://doi.org/10.1063/1.1137153.
Falk, M.L., Langer, J.S., 1998. Dynamics of viscoplastic deformation in amorphous solids. Phys. Rev. E 57, 7192-7205. https://doi.org/10.1103/PhysRevE.57.7192.
Feng, S.D., Qi, L., Wang, L.M., Yu, P.F., Zhang, S.L., Ma, M.Z., Zhang, X.Y., Jing, Q., Ngai, K.L., Greer, A.L., Li, G., Liu, R.P., 2016. Structural feature of Cu64Zr36 metallic glass on nanoscale: Densely-packed clusters with loosely-packed surroundings. Scr. Mater 115, 57-61. https://doi.org/https://doi.org/10.1016/j.scriptamat.2015.12.038.
Ferry, J.D., 1980. Viscoelastics properties of polymers. New York:Wiley.
Gadaud, P., Pautrot, S., 2003. Characterization of the elasticity and anelasticity of bulk glasses by dynamical subresonant and resonant techniques. J. Non·Cryst. Solids 316, 146-152. https://doi.org/10.1016/S0022-3093(02)01947-6.
Geirhos, K., Lunkenheimer, P., Loidl, A., 2018. Johari-Goldstein Relaxation Far Below ${T}_{g}$: Experimental Evidence for the Gardner Transition in Structural Glasses? Phys. Rev. Lett. 120, 085705. https://doi.org/10.1103/PhysRevLett.120.085705.
Granato, A.V., 2014. Interstitialcy theory of simple condensed matter. Eur. Phys. J. B 87, 18. https://doi.org/10.1140/epjb/e2013-41024-1.
Huang, R., Suo, Z., Prevost, J.H., Nix, W.D., 2002. Inhomogeneous deformation in metallic glasses. J. Mech. Phys. Solids 50, 1011-1027. https://doi.org/10.1016/S0022-5096(01)00115-6.
Hufnagel, T.C., Schuh, C.A., Falk, M.L., 2016. Deformation of metallic glasses: Recent developments in theory, simulations, and experiments. Acta Mater. 109, 375-393. https://doi.org/10.1016/j.actamat.2016.01.049.
Huo, L.S., Zeng, J.F., Wang, W.H., Liu, C.T., Yang, Y., 2013. The dependence of shear modulus on dynamic relaxation and evolution of local structural heterogeneity in a metallic glass. Acta Mater. 61, 4329-4338. https://doi.org/10.1016/j.actamat.2013.04.004.
Inoue, A., Takeuchi, A., 2011. Recent development and application products of bulk glassy alloys. Acta Mater. 59, 2243-2267. https://doi.org/10.1016/j.actamat.2010.11.027.
Jiang, H.Y., Luo, P., Wen, P., Bai, H.Y., Wang, W.H., Pan, M.X., 2016. The near constant loss dynamic mode in metallic glass. J. Appl. Phys. 120, 6. https://doi.org/10.1063/1.4964809.
Jiang, S.S., Gan, K.F., Huang, Y.J., Xue, P., Ning, Z.L., Sun, J.F., Ngan, A.H.W., 2020. Stochastic deformation and shear transformation zones of the glassy matrix in CuZr-based metallic-glass composites. Int. J. Plast 125, 52-62. https://doi.org/10.1016/

j.ijplas.2019.09.005.
Johari, G.P., 1973. Intrinsic mobility of molecular glasses. J. Chem. Phys. 58, 1766-1770. https://doi.org/10.1063/1.1679421.
Johnson, W.L., Samwer, K., 2005. A universal criterion for plastic yielding of metallic glasses with a (T/T-g)(2/3) temperature dependence. Phys. Rev. Lett. 95, 4. https://doi.org/10.1103/PhysRevLett.95.195501.
Ju, J.D., Jang, D., Nwankpa, A., Atzmon, M., 2011. An atomically quantized hierarchy of shear transformation zones in a metallic glass. J. Appl. Phys. 109, 053522. https://doi.org/10.1063/1.3552300.
Ke, H.B., Zeng, J.F., Liu, C.T., Yang, Y., 2014. Structure Heterogeneity in Metallic Glass: Modeling and Experiment. J. Mater. Sci. Technol. 30, 560-565. https://doi.org/10.1016/j.jmst.2013.11.014.
Khmich, A., Hassani, A., Sbiaai, K., Hasnaoui, A., 2021. Tuning of mechanical properties of Tantalum-based metallic glasses. Int. J. Mech. Sci., 106546. https://doi.org/10.1016/j.ijmecsci.2021.106546.
Langer, J.S., 2015. Shear-transformation-zone theory of yielding in athermal amorphous materials. Phys. Rev. E 92, 012318. https://doi.org/10.1103/PhysRevE.92.012318.
Lei, T.J., DaCosta, L.R., Liu, M., Shen, J., Sun, Y.H., Wang, W.H., Atzmon, M., 2020. Composition dependence of metallic glass plasticity and its prediction from anelastic relaxation – A shear transformation zone analysis. Acta Mater. 195, 81-86. https://doi.org/10.1016/j.actamat.2020.04.053.
Li, L., Homer, E.R., Schuh, C.A., 2013. Shear transformation zone dynamics model for metallic glasses incorporating free volume as a state variable. Acta Mater. 61, 3347-3359. https://doi.org/10.1016/j.actamat.2013.02.024.
Li, Z.J., Liu, Z.L., Zhuang, Z., Cui, Y.N., 2021. Temperature dependent deformation localization in irradiated tungsten. Int. J. Plast 146, 103077. https://doi.org/10.1016/j.ijplas.2021.103077.
Lin, W.-H., Teng, Y., Sha, Z.-D., Yuan, S.-Y., Branicio, P.S., 2020. Mechanical properties of nanoporous metallic glasses: Insights from large-scale atomic simulations. Int. J. Plast 127, 102657. https://doi.org/10.1016/j.ijplas.2019.102657.
Liu, Y.H., Wang, D., Nakajima, K., Zhang, W., Hirata, A., Nishi, T., Inoue, A., Chen, M.W., 2011. Characterization of nanoscale mechanical heterogeneity in a metallic glass by dynamic force microscopy. Phys. Rev. Lett. 106, 125504. https://doi.org/10.1103/PhysRevLett.106.125504.
Luckabauer, M., Hayashi, T., Kato, H., Ichitsubo, T., 2019. Decreasing activation energy of fast relaxation processes in a metallic glass during aging. Phys. Rev. B 99, 140202. https://doi.org/10.1103/PhysRevB.99.140202.
Luo, P., Wen, P., Bai, H.Y., Ruta, B., Wang, W.H., 2017. Relaxation decoupling in metallic glasses at low temperatures. Phys. Rev. Lett. 118, 225901. https://doi.org/10.1103/PhysRevLett.118.225901.
McElfresh, C., Cui, Y.N., Dudarev, S.L., Po, G., Marian, J., 2021. Discrete stochastic model of point defect-dislocation interaction for simulating dislocation climb. Int. J. Plast 136, 19. https://doi.org/10.1016/j.ijplas.2020.102848.

Menard, K.P., 2015. Dynamic mechanical analysis, Third Edition. Crc Press.
Mitrofanov, Y.P., Wang, D.P., Makarov, A.S., Wang, W.H., Khonik, V.A., 2016. Towards understanding of heat effects in metallic glasses on the basis of macroscopic shear elasticity. Sci. Rep 6, 23026. https://doi.org/10.1038/srep23026.
Ngai, K.L., Wang, L.M., Yu, H.B., 2017. Relating ultrastable glass formation to enhanced surface diffusion via the Johari-Goldstein beta-relaxation in molecular glasses. J. Phys. Chem. Lett. 8, 2739-2744. https://doi.org/10.1021/acs.jpclett.7b01192.
Nomoto, K., Ceguerra, A.V., Gammer, C., Li, B., Bilal, H., Hohenwarter, A., Gludovatz, B., Eckert, J., Ringer, S.P., Kruzic, J.J., 2021. Medium-range order dictates local hardness in bulk metallic glasses. Mater. Today 44, 48-57. https://doi.org/10.1016/j.mattod.2020.10.032.
Olsen, N.B., Christensen, T., Dyre, J.C., 2001. Time-temperature superposition in viscous liquids. Phys. Rev. Lett. 86, 1271-1274. https://doi.org/10.1103/PhysRevLett.86.1271.
Palmer, R.G., Stein, D.L., Abrahams, E., Anderson, P.W., 1984. Models of hierarchically constrained dynamics for glassy relaxation. Phys. Rev. Lett. 53, 958-961. https://doi.org/10.1103/PhysRevLett.53.958.
Pan, J., Zhou, H.F., Wang, Z.T., Li, Y., Gao, H.J., 2015. Origin of anomalous inverse notch effect in bulk metallic glasses. J. Mech. Phys. Solids 84, 85-94. https://doi.org/10.1016/j.jmps.2015.07.006.
Pelletier, J.M., Perez, J., Duffrene, L., 2000. Mechanical response of an oxide glass to mechanical loading - Shear and volume relaxation effects: Physical analysis. Acta Mater. 48, 1397-1408. https://doi.org/10.1016/s1359-6454(99)00387-0.
Perez, J., 1984. Homogeneous flow and anelastic/plastic deformation of metallic glasses. Acta Metall. 32, 2163-2173. https://doi.org/10.1016/0001-6160(84)90159-7.
Perez, J., 1990. Quasi-punctual defects in vitreous solids and liquid-glass transition. Solid State Ionics 39, 69-79. https://doi.org/10.1016/0167-2738(90)90028-P.
Perez, J., 1998. Physics and mechanics of amorphous polymers. CRC Press.
Perez, J., Cavaille, J.Y., Etienne, S., Jourdan, C., 1988. Physical interpretation of the rheological behavior of amorphous polymers through the glass-transition. Rev. Phys. Appl. 23, 125-135. https://doi.org/10.1051/rphysap:01988002302012500.
Po, G., Cui, Y.N., Rivera, D., Cereceda, D., Swinburne, T.D., Marian, J., Ghoniem, N., 2016. A phenomenological dislocation mobility law for bcc metals. Acta Mater. 119, 123-135. https://doi.org/10.1016/j.actamat.2016.08.016.
Qiao, J., Chen, Y., Casalini, R., Pelletier, J., Yao, Y., 2019a. Main α relaxation and slow β relaxation processes in a La30Ce30Al15Co25 metallic glass. J. Mater. Sci. Technol. 35, 982-986. https://doi.org/10.1016/j.jmst.2018.12.003.
Qiao, J., Pelletier, J.M., 2014. Dynamic mechanical relaxation in bulk metallic glasses: A review. J. Mater. Sci. Technol. 30, 523-545. https://doi.org/10.1016/j.jmst.2014.04.018.
Qiao, J.C., Pelletier, J.M., Yao, Y., 2019b. Creep in bulk metallic glasses. Transition from linear to non linear regime. Mater. Sci. Eng., A 743, 185-189. https://doi.org/10.1016/j.msea.2018.11.066.
Qiao, J.C., Wang, Q., Crespo, D., Yang, Y., Pelletier, J.M., 2017. Amorphous physics

and materials: Secondary relaxation and dynamic heterogeneity in metallic glasses: A brief review. Chin. Phys. B 26, 016402. https://doi.org/10.1088/1674-1056/26/1/016402.
Qiao, J.C., Wang, Q., Pelletier, J.M., Kato, H., Casalini, R., Crespo, D., Pineda, E., Yao, Y., Yang, Y., 2019c. Structural heterogeneities and mechanical behavior of amorphous alloys. Prog. Mater. Sci. 104, 250-329. https://doi.org/10.1016/j.pmatsci.2019.04.005.
Qiao, J.C., Wang, Y.-J., Zhao, L.Z., Dai, L.H., Crespo, D., Pelletier, J.M., Keer, L.M., Yao, Y., 2016a. Transition from stress-driven to thermally activated stress relaxation in metallic glasses. Phys. Rev. B 94, 104203. https://doi.org/10.1103/PhysRevB.94.104203.
Qiao, J.C., Wang, Y.J., Pelletier, J.M., Keer, L.M., Fine, M.E., Yao, Y., 2015. Characteristics of stress relaxation kinetics of $La_{60}Ni_{15}Al_{25}$ bulk metallic glass. Acta Mater. 98, 43-50. https://doi.org/10.1016/j.actamat.2015.07.020.
Qiao, J.C., Yao, Y., Pelletier, J.M., Keer, L.M., 2016b. Understanding of micro-alloying on plasticity in Cu46Zr47−xAl7Dyx ($0 \leq x \leq 8$) bulk metallic glasses under compression: Based on mechanical relaxations and theoretical analysis. Int. J. Plast 82, 62-75. https://doi.org/10.1016/j.ijplas.2016.02.002.
Rinaldi, R., Gaertner, R., Chazeau, L., Gauthier, C., 2011. Modelling of the mechanical behaviour of amorphous glassy polymer based on the Quasi Point Defect theory—Part I: Uniaxial validation on polycarbonate. Int. J. Non-Linear Mech. 46, 496-506. https://doi.org/10.1016/j.ijnonlinmec.2010.11.004.
Ruan, D., Patinet, S., Falk, M.L., 2022. Predicting plastic events and quantifying the local yield surface in 3D model glasses. J. Mech. Phys. Solids 158, 104671. https://doi.org/10.1016/j.jmps.2021.104671.
Schall, P., Weitz, D.A., Spaepen, F., 2007. Structural rearrangements that govern flow in colloidal glasses. Science 318, 1895-1899. https://doi.org/10.1126/science.1149308.
Schuh, C.A., Hufnagel, T.C., Ramamurty, U., 2007. Mechanical behavior of amorphous alloys. Acta Mater. 55, 4067-4109. https://doi.org/10.1016/j.actamat.2007.01.052.
Schuh, C.A., Mason, J.K., Lund, A.C., 2005. Quantitative insight into dislocation nucleation from high-temperature nanoindentation experiments. Nat. Mater 4, 617-621. https://doi.org/10.1038/nmat1429.
Sha, Z.D., Teng, Y., Poh, L.H., Pei, Q.X., Xing, G.C., Gao, H.J., 2019. Notch strengthening in nanoscale metallic glasses. Acta Mater. 169, 147-154. https://doi.org/10.1016/j.actamat.2019.02.044.
Shang, B.S., Rottler, J., Guan, P.F., Barrat, J.L., 2019. Local versus global stretched mechanical response in a supercooled liquid near the glass transition. Phys. Rev. Lett. 122, 5. https://doi.org/10.1103/PhysRevLett.122.105501.
Shi, Y.F., Falk, M.L., 2007. Stress-induced structural transformation and shear banding during simulated nanoindentation of a metallic glass. Acta Mater. 55, 4317-4324. https://doi.org/10.1016/j.actamat.2007.03.029.
Singh, I., Guo, T.F., Murali, P., Narasimhan, R., Zhang, Y.W., Gao, H.J., 2013. Cavitation in materials with distributed weak zones: Implications on the origin of brittle fracture in metallic glasses. J. Mech. Phys. Solids 61, 1047-1064. https://doi.org/10.1016/j.jmps.2012.12.001.

Song, J., Zhu, W., Wei, X., 2021. Correlations between the hierarchical spatial heterogeneity and the mechanical properties of metallic glasses. Int. J. Mech. Sci. 204, 106570. https://doi.org/10.1016/j.ijmecsci.2021.106570.
Soriano, D., Zhou, H., Hilke, S., Pineda, E., Ruta, B., Wilde, G., 2021. Relaxation dynamics of Pd–Ni–P metallic glass: decoupling of anelastic and viscous processes. J. Phys.: Condens. Matter 33, 164004. https://doi.org/10.1088/1361-648x/abef27.
Spaepen, F., 1977. A microscopic mechanism for steady state inhomogeneous flow in metallic glasses. Acta Metall. 25, 407-415. https://doi.org/10.1016/0001-6160(77)90232-2.
Spaepen, F., 1978. Structural imperfections in amorphou metals. J. Non·Cryst. Solids 31, 207-221. https://doi.org/10.1016/0022-3093(78)90105-9.
Srolovitz, D., Maeda, K., Vitek, V., Egami, T., 1981. Structural defects in amorphous solids Statistical analysis of a computer model. Philos. Mag. A 44, 847-866. https://doi.org/10.1080/01418618108239553.
Stukowski, A., Cereceda, D., Swinburne, T.D., Marian, J., 2015. Thermally-activated non-Schmid glide of screw dislocations in W using atomistically-informed kinetic Monte Carlo simulations. Int. J. Plast 65, 108-130. https://doi.org/10.1016/j.ijplas.2014.08.015.
Sun, B.A., Song, K.K., Pauly, S., Gargarella, P., Yi, J., Wang, G., Liu, C.T., Eckert, J., Yang, Y., 2016. Transformation-mediated plasticity in CuZr based metallic glass composites: A quantitative mechanistic understanding. Int. J. Plast 85, 34-51. https://doi.org/10.1016/j.ijplas.2016.06.004.
Tang, C.G., Harrowell, P., 2013. Anomalously slow crystal growth of the glass-forming alloy CuZr. Nat. Mater 12, 507-511. https://doi.org/10.1038/nmat3631.
Tong, X., Wang, G., Yi, J., Ren, J.L., Pauly, S., Gao, Y.L., Zhai, Q.J., Mattern, N., Dahmen, K.A., Liaw, P.K., Eckert, J., 2016. Shear avalanches in plastic deformation of a metallic glass composite. Int. J. Plast 77, 141-155. https://doi.org/10.1016/j.ijplas.2015.10.006.
Tsai, P., Kranjc, K., Flores, K.M., 2017. Hierarchical heterogeneity and an elastic microstructure observed in a metallic glass alloy. Acta Mater. 139, 11-20. https://doi.org/10.1016/j.actamat.2017.07.061.
Turnbull, D., Cohen, M.H., 1970. On the free-volume model of the iquid-glass transition. J. Chem. Phys. 52, 3038-3041. https://doi.org/10.1063/1.1673434.
Van Loock, F., Brassart, L., Pardoen, T., 2021. Implementation and calibration of a mesoscale model for amorphous plasticity based on shear transformation dynamics. Int. J. Plast 145, 103079. https://doi.org/10.1016/j.ijplas.2021.103079.
Wang, Q., Liu, J.J., Ye, Y.F., Liu, T.T., Wang, S., Liu, C.T., Lu, J., Yang, Y., 2017. Universal secondary relaxation and unusual brittle-to-ductile transition in metallic glasses. Mater. Today 20, 293-300. https://doi.org/10.1016/j.mattod.2017.05.007.
Wang, Q., Pelletier, J.M., Lu, J., Dong, Y.D., 2005. Study of internal friction behavior in a Zr base bulk amorphous alloy around the glass transition. Mater. Sci. Eng., A 403, 328-333. https://doi.org/10.1016/j.msea.2005.05.014.
Wang, W.H., 2012. The elastic properties, elastic models and elastic perspectives of metallic glasses. Prog. Mater. Sci. 57, 487-656. https://doi.org/10.1016/

j.pmatsci.2011.07.001.
Wang, Z., Wang, W.-H., 2019. Flow units as dynamic defects in metallic glassy materials. Natl. Sci. Rev. 6, 304-323. https://doi.org/10.1093/nsr/nwy084.
Xie, X., Lo, Y.C., Tong, Y., Qiao, J.W., Wang, G.Y., Ogata, S., Qi, H.R., Dahmen, K.A., Gao, Y.F., Liaw, P.K., 2019. Origin of serrated flow in bulk metallic glasses. J. Mech. Phys. Solids 124, 634-642. https://doi.org/10.1016/j.jmps.2018.11.015.
Xu, B., Falk, M.L., Li, J.F., Kong, L.T., 2018. Predicting Shear Transformation Events in Metallic Glasses. Phys. Rev. Lett. 120, 125503. https://doi.org/10.1103/PhysRevLett.120.125503.
Yang, Y., Zeng, J.F., Volland, A., Blandin, J.J., Gravier, S., 2012a. Fractal growth of the dense-packing phase in annealed metallic glass imaged by high-resolution atomic force microscopy. Acta Mater. 60, 5260-5272. https://doi.org/10.1016/j.actamat.2012.06.025.
Yang, Y., Zeng, J.F., Volland, A., Blandin, J.J., Gravier, S., Liu, C.T., 2012b. Fractal growth of the dense-packing phase in annealed metallic glass imaged by high-resolution atomic force microscopy. Acta Mater. 60, 5260-5272. https://doi.org/10.1016/j.actamat.2012.06.025.
Yang, Y., Zhou, J., Zhu, F., Yuan, Y., Chang, D.J., Kim, D.S., Pham, M., Rana, A., Tian, X., Yao, Y., Osher, S.J., Schmid, A.K., Hu, L., Ercius, P., Miao, J., 2021. Determining the three-dimensional atomic structure of an amorphous solid. Nature 592, 60-64. https://doi.org/10.1038/s41586-021-03354-0.
Ye, J.C., Lu, J., Liu, C.T., Wang, Q., Yang, Y., 2010. Atomistic free-volume zones and inelastic deformation of metallic glasses. Nat. Mater 9, 619-623. https://doi.org/10.1038/nmat2802.
Yu, H.B., Richert, R., Samwer, K., 2017. Structural rearrangements governing Johari-Goldstein relaxations in metallic glasses. Sci. Adv. 3, e1701577. https://doi.org/10.1126/sciadv.1701577.
Yu, H.B., Wang, W.H., Bai, H.Y., Samwer, K., 2014. The β-relaxation in metallic glasses. Natl. Sci. Rev. 1, 429-461. https://doi.org/10.1093/nsr/nwu018.
Yu, Q., Chatterjee, S., Roche, K.J., Po, G., Marian, J., 2021. Coupling crystal plasticity and stochastic cluster dynamics models of irradiation damage in tungsten. Modelling Simul. Mater. Sci. Eng. 29, 055021. https://doi.org/10.1088/1361-651x/ac01ba.
Zhang, M., Chen, Y., Li, W., 2019. On the origin of softening in the plastic deformation of metallic glasses. Int. J. Plast 116, 24-38. https://doi.org/10.1016/j.ijplas.2018.12.004.
Zhang, P., Maldonis, J.J., Liu, Z., Schroers, J., Voyles, P.M., 2018. Spatially heterogeneous dynamics in a metallic glass forming liquid imaged by electron correlation microscopy. Nat. Commun. 9, 1129. https://doi.org/10.1038/s41467-018-03604-2.
Zhao, L.Z., Xue, R.J., Zhu, Z.G., Ngai, K.L., Wang, W.H., Bai, H.Y., 2016. A fast dynamic mode in rare earth based glasses. J. Chem. Phys. 144, 204507. https://doi.org/10.1063/1.4952421.
Zhou, H.F., Qu, S.X., Yang, W., 2013. An atomistic investigation of structural evolution in metallic glass matrix composites. Int. J. Plast 44, 147-160. https://doi.org/10.1016/j.ijplas.2013.01.002.
Zhu, F., Song, S.X., Reddy, K.M., Hirata, A., Chen, M.W., 2018. Spatial heterogeneity

as the structure feature for structure–property relationship of metallic glasses. Nat. Commun. 9, 3965. https://doi.org/10.1038/s41467-018-06476-8.
Zhu, W.Q., Liu, J.J., Mao, S., Wei, X.D., 2021. A new continuum model for viscoplasticity in metallic glasses based on thermodynamics and its application to creep tests. J. Mech. Phys. Solids 146. https://doi.org/10.1016/j.jmps.2020.104216.
Zhu, Z.G., Wen, P., Wang, D.P., Xue, R.J., Zhao, D.Q., Wang, W.H., 2013. Characterization of flow units in metallic glass through structural relaxations. J. Appl. Phys. 114, 083512. https://doi.org/10.1063/1.4819484.